Pergamon

0277-5387(95)00064-X

*Polyhedron* Vol. 14, No. 22, pp. 3335–3362, 1995

0277-5387/95 $9.50+0.00

# CHEMISTRY OF ELECTROPHILIC METAL CENTRES COORDINATED BY SILOX ($^t$Bu$_3$SiO), TRITOX ($^t$Bu$_3$CO) AND RELATED BINFUNCTIONAL LIGANDS

PETER T. WOLCZANSKI

Cornell University, Baker Laboratory, Department of Chemistry, Ithaca, NY 14853, U.S.A.

**Abstract**—Bulky siloxide and alkoxide ligands, notably silox ($^t$Bu$_3$SiO), and tritox ($^t$Bu$_3$CO), have been employed as ancillary ligands in the chemistry of low-coordinate early transition metal complexes. Related sterically hindered difunctional ligands (e.g., alkoxyalkylphosphines) are utilized to link disparate early and late transition metal centres together in a quest for cooperative reactivity. This review focuses on our group's efforts in this area over the past 14 years. Emphasis is placed on the rationale for using bulky, hard, anionic donor ligands, and the synthesis and reactivity studies of this class of compounds.

## INTRODUCTION

### *Alkoxides as cyclopentadienyl replacements*

At Cornell University in 1981, we initiated a program emphasizing the development of alkoxide ligands as alternatives to cyclopentadienyl. Cyclopentadienyl (Cp = $\eta^5$-$C_5H_5$), ubiquitous in every niche of organometallic chemistry,[1] was an obvious, yet challenging target for mimicry. Since Cp is a strong, 5e$^-$ donor (the neutral counting method will be used throughout), its replacement by sterically equivalent, lesser donating alkoxide ligands would enable the preparation of complexes possessing inherent electronic unsaturation; as a consequence, these compounds would surely exhibit greater reactivity.

The concept of using bulky ligands to generate low coordinate, reactive metal centres is as old as an understanding of the EAN or 16/18e$^-$ rule. With few exceptions, a metal centre must by necessity bind a substrate while transforming it, hence the preparation of complexes with electron counts of less than 16/18e$^-$ has historically commanded much attention.[1] Complexes containing bulky neutral ligands, such as $PR_3$ (e.g. R = $^i$Pr, Cy, $^t$Bu) and $\pi$-hydrocarbons, both neutral (e.g. $\eta^6$-$C_6R_6$) and anionic (e.g. Cp* = $\eta^5$-$C_5Me_5$, $\eta^8$-$C_8H_8$), have been the primary targets of this approach. The use of anionic ligands that can be construed as strong $p\pi$-donors, especially those containing electronegative donor atoms such as oxygen and nitrogen, has been less evident. In 1981, the chemistry of smaller O- and N-donors was being explored, and intriguing results were forthcoming, but very few could be considered as *bona fide* cyclopentadienyl alternatives in the manner that we envisioned when our program began. Nonetheless, one need only examine the early chemistry of the $(Me_3Si)_2N^-$ and related bulky amide ligands[2,3] in order for the exploration of related alkoxide or siloxide ligation to gain credence.

### *Steric aspects of alkoxides and siloxides*

Estimates by Tolman[4] placed the cone angle of cyclopentadienyl at roughly 136°. Related measurements in these laboratories implicated a smaller cone angle as more realistic (~130°) for Cp, but it was clear that any alkoxide analogue would necessitate the use of a group substantially greater in size than $^t$Bu (cone angle of $^t$BuO$^-$ < 90°). An alkoxide has only one substituent on the heteroatom, in contrast to hindered amides [e.g. $(Me_3Si)_2N^-$], and its bulk is centred two bond lengths from the metal, hence it must be extremely large if steric control of reactivity is a primary goal.

As Fig. 1 illustrates, the substituent must also be able to reproduce and fill a true conical region of space, just like Cp. Rothwell had embarked on a related program investigating early transition metals ligated by bulky phenoxide ligands, principally 2,6-substituted derivatives. His initial entry into group 4 yielded tris-aryloxide derivatives of zirconium that were prepared regardless of the initial $ZrCl_4/ArO^-$ stoichiometry.[5] We viewed an aryloxide ligand as wedge-like in shape, similar to its predecessor $(Me_3Si)_2N^-$; as a consequence, it can pack efficiently about a metal centre despite the typical bulky $^t$Bu or $^i$Pr groups in the *ortho* positions on the ring. The ready formation of tris-aryloxide derivatives in this early work may be attributed to the packing ability of these wedges.

Our focus centred on ligands that would occupy a regular cone of space about the metal, just as in symmetric cyclopentadienyl derivatives. We sought bulky alkoxides or siloxides that possessed three equivalent bulky R groups triangulated about the O—C(Si) vector.

*Alkoxide and siloxide electronic features*

In principle, alkoxide and cyclopentadienyl ligands are electronically analogous. Linear combinations of C $\pi$-orbitals comprise $\sigma$- and $\pi$-donor orbitals of cyclopentadienyl, as illustrated in Fig. 2, while an alkoxide or siloxide ligand binds principally through a $\sigma$-type orbital, such as the *sp* hybrid indicated, and via $\pi$-donation of two $p\pi$-orbitals that are perpendicular to the M—O vector. In converting from a molecular orbital depiction to simple EAN counting, it can be inferred that an alkoxide or siloxide can be a $5e^-$ donor akin to cyclopentadienyl, but how realistic is this assessment?

It is impossible to quantify the number of electrons donated to the metal without some concrete definition of how charge distribution is to be assigned, hence the organometallic community often relies on structural information to support

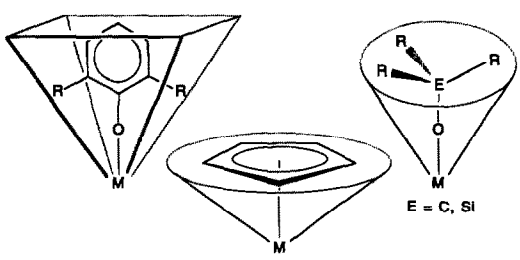


Fig. 1. Spatial perceptions of an aryloxide "wedge" and the conical displacements of Cp and a triangulated alkoxide or siloxide.

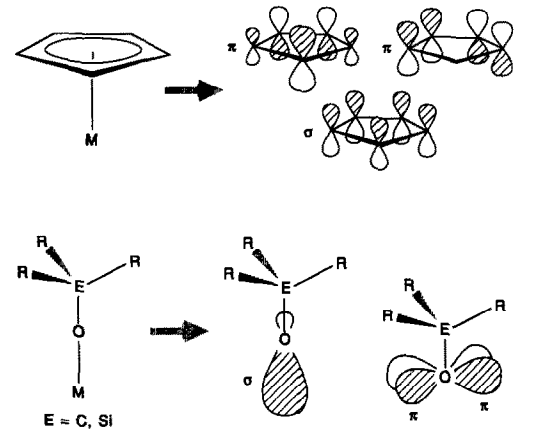


Fig. 2. Donor orbital analogy of Cp to an alkoxide $(\sigma+2\pi)$.

the claims of multiple metal–ligand bonding. Here Rothwell has provided an analysis that cautions against the overinterpretation of structural data.[6] The angle of the M—O—C linkage and the metal–oxygen bond length are the typical criteria for assessing metal alkoxide bond order. An M—O—C bond angle that is near linearity indicates significant involvement of both $p\pi$-orbitals in $O(p\pi) \rightarrow M(d\pi)$ donation; the shorter the M—O bond, the stronger the interaction. However, Rothwell has shown that there is little, if any, correlation between M—O—C bond angle and $d$(M—O)!

The energy match between the metal $\sigma$- and $\pi$-acceptor orbitals in comparison to the donor orbitals of the alkoxide, and the critical orbital overlaps—i.e. the basis of a first-order perturbation theory treatment of metal–ligand interactions—need to be evaluated for proper assessment of the metal–ligand interaction. Rudimentary Extended Hückel Molecular Orbital (EHMO) or higher level calculations can aid interpretations significantly. For the early metals, $O(p\pi) \rightarrow M(d\pi)$ interactions will tend to be stronger in the second and third rows, where the overlap of the appropriate orbitals is better than in the first row. This is counteracted to a lesser extent by a better energy match between the orbitals of the less electropositive first row metals and oxygen. On moving from left to right in the periodic table, orbital overlap declines, but the interacting orbitals approach one another energetically.

We have yet to observe chemistry that would suggest that an alkoxide or siloxide realistically manifests $5e^-$ donation, and typically view the RO ligand as a $3e^-$ donor, especially when conducting electron counting exercises. Two factors dominate our understanding of alkoxide and siloxide donation. First, $\sigma$-bonding for M—OR (M = early

metal) ligation is extremely strong, primarily due to the large ionic component of this formally covalent bond. We are often enamoured with assessing $\pi$-effects to the detriment of more important and sometimes subtler factors influencing $\sigma$-bonding. Second, the strength of both $\sigma$- and $\pi$-interactions depends on the electrophilicity of the metal centre. When required, as in the case of an extremely low-coordinate, electron-deficient centre, the strength of both types of interactions can increase to accommodate the metal. In this respect, just like any versatile ligand in organometallic chemistry, the typical alkoxide or siloxide can adapt to its environment.

On balance the use of a silyl, rather than alkyl, substituent on the oxygen renders the $R_3EO$ (E = C, Si) ligand less donating as a consequence of electrostatic effects. This is most easily seen in examination of the $pK_a$ values of related species. For example, $Ph_3SiOH$ ($pK_a$ = 16.57, DMSO) exhibits a higher acid dissociation constant than $Ph_3COH$ ($pK_a$ = 16.97, DMSO),[7] reflecting the inductive influence of the more electropositive silicon. Relative to alkoxides, less basic siloxide ligands bind to a metal with slightly more ionic character. An $R_3Si$ group possesses fairly low-lying, empty $3d/\sigma^*$ fragment molecular orbitals that can interact with $p\pi$-orbitals of oxygen. The minor $\pi$-accepting capability of silicon, whose significance has been disputed,[8] is thought to attenuate the $O(p\pi) \rightarrow M(d\pi)$ donation usually ascribed to the ROM unit. The general electronic consequences of utilizing a siloxide rather than alkoxide ligand are manifested in a greater electrophilicity at the metal centre. While pertinent spectroscopic information is limited, siloxide ligands are believed to electronically influence a metal centre in roughly the same manner as aryloxides;[9] both are substantially better at supporting reduced metal centres. Such observations lead one to a simplified description of siloxides as pseudohalides—pseudohalides with adjustable steric parameters.

## TRITOX, SILOX AND RELATED BIFUNCTIONAL LIGANDS

### *Tritox* ($^t Bu_3CO^-$)

*Synthesis.* The first ligand utilized in our program—and one still being applied in select circumstances—was tri-tert-butylmethoxide ($^t Bu_3CO^-$), coined tritox (Fig. 3) by M. L. H. Green. Its original synthesis by Bartlett at Harvard[10] has been slightly modified by Syper.[11] The result is a one-step procedure whereby $^t$BuLi is added to methylpivalate to afford a mixture of

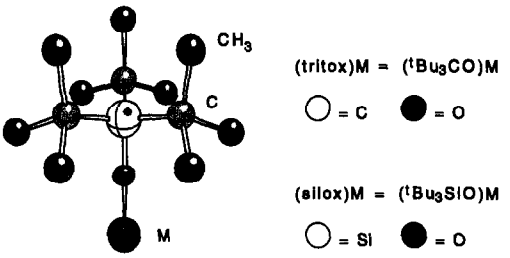


Fig. 3. The tri-tert-butyl cones of tritox ($^t Bu_3CO^-$) and silox ($^t Bu_3SiO^-$).

$^t Bu_3COH$ and $^t Bu_2CHOH$ (eq. 1). Distillation under reduced pressure removes most of the

$$^t BuC(O)OMe + 2\,^t BuLi \xrightarrow[\text{hexane}]{\text{(1) } -78\ ^\circ C} {}^t Bu_3COH + {}^t Bu_2CHOH \quad (1)$$
$$\text{(2) } H^+, H_2O$$

$^t Bu_2CHOH$, and pure $^t Bu_3COH$ (60–70%, m.p. 105–110°C) may be obtained upon crystallization from MeOH. Deprotonation to provide Li(tritox) ($^t Bu_3COLi$) was typically accomplished with $^n$BuLi in 91% isolated yield.[12] Other anion equivalents were also prepared, but the lithium derivative proved suitable for most metathetical transformations.

*Steric aspects of metathesis.* When attached to a metal, tritox occupies a symmetric, approximately 125° cone of space; consequently, some steric control of halide substitution can be observed. Treatment of $ZrCl_4$ with 2 equiv. Li(tritox) afforded $(tritox)_2ZrCl_3 \cdot Li(OE_2)_2$ (**1**) in 80% yield according to eq. (2); subsequent dissolution, filtration and

$$ZrCl_4 + 2Li(tritox) \xrightarrow[8\text{ h}, -LiCl]{Et_2O,\ 25\ ^\circ C} (tritox)_2ZrCl_3 \cdot Li(OEt_2)_2 \quad (2)$$
$$\mathbf{1}$$

$$(tritox)_2ZrCl_3 \cdot Li(OEt_2) \xrightarrow[-LiCl]{hexane} (tritox)_2ZrCl_2 \quad (3)$$
$$\mathbf{1} \qquad\qquad \mathbf{2}$$

crystallization from hexane provided the bis-alkoxide derivative, $(tritox)_2ZrCl_2$ (**2**, eq. 3). Disproportionation of **2**, a mimic of $Cp_2ZrCl_2$, was not evident, although ligand degradation (*vide infra*) proved problematic.

With titanium ($r_{cov} \sim 1.32$ Å), a mono-tritox complex, $(tritox)TiCl_3$ (**3**), was prepared upon addition of Li(tritox) to $TiCl_4$ in $Et_2O$ (57%, eq. 4), further proof that steric control of metathetical

$$TiCl_4 + Li(tritox) \xrightarrow[1\,h,\,-LiCl]{Et_2O,\,-78^\circ C} \underset{\mathbf{3}}{(tritox)TiCl_3} \quad (4)$$

$$TiCl_4 + 2\,Li(tritox) \xrightarrow[6\,h,\,-2\,LiCl]{Et_2O,\,-78^\circ C} \underset{\mathbf{4}}{(tritox)_2TiCl_2} \quad (5)$$

processes was possible in certain instances; $(tritox)_2TiCl_2$ (**4**) was easily prepared (60% yield) from 2 equiv. of Li(tritox). In contrast, difficulties were encountered when mono-tritox derivatives of zirconium, which has a covalent radius substantially larger ($r_{cov} \sim 1.45$ Å) than titanium, were the synthetic targets. Alcoholysis of $ZrR_4$ (R = $CH_2Ph$, $CH_2{}^tBu$) proved necessary to prepare $(tritox)ZrR_3$ (**5**, R = $CH_2Ph$, 82%; **6**, R = $CH_2{}^tBu$, 16%). Conditions were severe in the case of **6**; a 30 h thermolysis (95°C) of virtually neat H(tritox) and $Zr(CH_2{}^tBu)_4$ with a trace of benzene was required.

$$ZrR_4 + H(tritox) \xrightarrow[benzene]{\Delta} (tritox)ZrR_3 \quad (6)$$

R = $CH_2Ph$, **5**; $CH_2{}^tBu$, **6**

*Tritox degradation.* While the Ti and Zr chloride complexes above were at least metastable, application of standard metathetical reactions toward tantalum and niobium proved fruitless.[13] Unfortunately, when bound to a metal that contained heterolytically labile ligands (e.g. halides), tritox decomposed to products derived from $^tBu_3C^+$. Bartlett *et al.*[10] and later investigations deemed this process to be interesting physical organic chemistry, but we did not concur! Scheme 1 illustrates how heterolytic cleavage of the tritox C—O bond may occur, ultimately leading to a pair of olefins and $H^+$.[12] Protons generated in this fashion provide a ready pathway for autocatalytic decomposition, as qualitative rates of degradation appear to show. As predicted, alkylation afforded complexes whose thermal stability was increased dramatically relative to the halides. While $(tritox)_2ZrCl_2$ (**2**) degraded within 24 h at 25°C in $C_6D_6$, the corresponding dimethyl, $(tritox)_2ZrMe_2$, exhibited only ~20% decomposition after 3 weeks at 100°C in $C_6D_6$. The tritox titanium chlorides possessed greater stability than zirconium, presumably because of a lesser $O(p\pi) \rightarrow M(d\pi)$ interaction due to worse orbital overlap. Nonetheless, both **3** and **4** degraded over a prolonged period of time and alkylation improved the stability of the Ti(tritox) linkage as well. Sen has elucidated related cationic alkoxide decomposition pathways in a concise, yet comprehensive, assessment of Ti—OR stability.[14] Stable tritox derivatives possessed excellent crystallinity on a macroscopic level, presumably due to the rigid, molecular framework of the tightly packed tert-butyl groups.

In an effort to stem heterolytic cleavage, 9-oxytriptycene (TpO) was employed as a ligand. The inability of C(9) to achieve planarity upon heterolysis was considered to obviate this degradation pathway. Unfortunately, while the stability of the ligand proved sufficient, the solubility of metal halide derivatives such as $(TpO)_2TaCl_3$ (**7**) was frustratingly low, even in DMSO. Alkylation of **7** with neopentyllithium, $^tBuCH_2Li$, afforded $(TpO)_2Ta(CH_2{}^tBu)_3$ (**8**, Scheme 2), a somewhat soluble hydrocarbon derivative that may be the most unreactive organometallic prepared in these laboratories; even hydrolysis proved to be incredibly slow

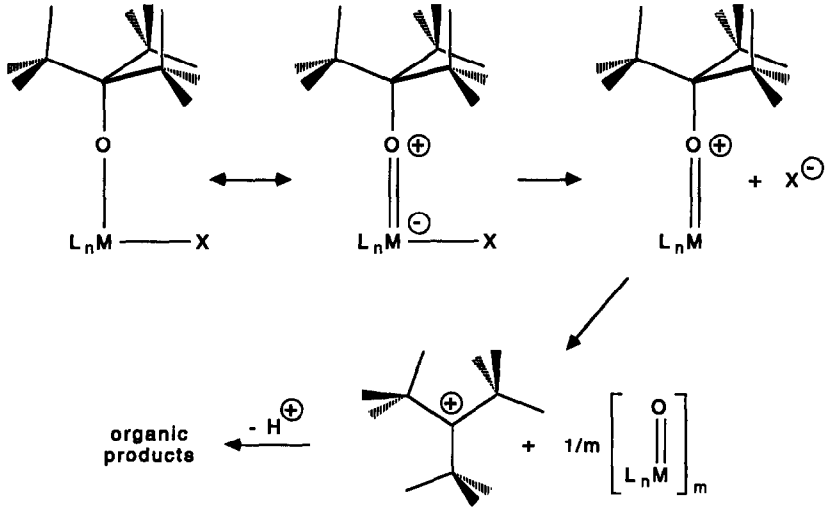


Scheme 1.

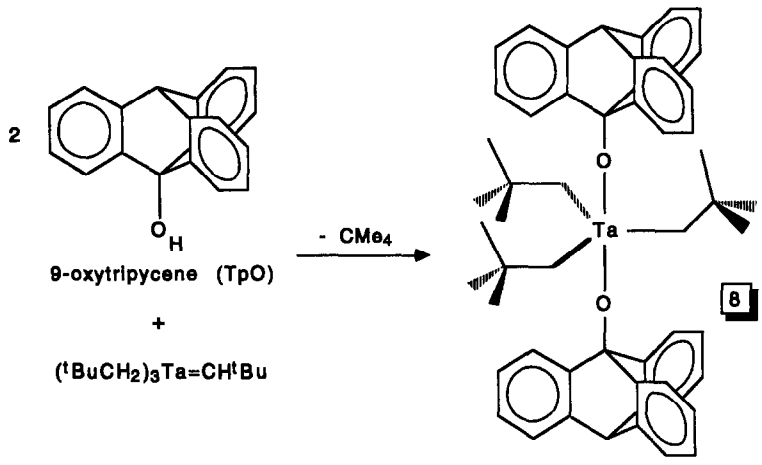


Scheme 2.

(120°C, $t_{1/2} \sim 12$ h; 12 M HCl, 25°C, $t_{1/2} \sim 0.5$ h) because the hydrocarbon periphery of the molecule, with the neopentyl ligands occupying the wedges between arene groups, was virtually impenetrable.

*Silox* ($^tBu_3SiO^-$)

*Synthesis.* The Dexheimer and Spialter preparation of $^tBu_3SiOH$ has proven to be the most useful, requiring sequential additions of $^t$BuLi to $SiF_4$ (60–70%) and $^tBu_2SiF_2$ (60–70%), followed by base hydrolysis of $^tBu_3SiH$ (~90%), as indicated in the following equations:[15]

$$SiF_4 + 2\,{}^t\text{BuLi} \xrightarrow{\text{hexane, 0°C}} {}^t\text{Bu}_2\text{SiF}_2 + 2\,\text{LiF} \quad (7)$$

$$^t\text{Bu}_2\text{SiF}_2 + 2\,{}^t\text{BuLi} \xrightarrow[70\text{–}80\,^\circ\text{C}]{\text{heptane, 3d}} {}^t\text{Bu}_3\text{SiH} + 2\,\text{LiF} + \text{Me}_2\text{C}{=}\text{CH}_2 \quad (8)$$

$$^t\text{Bu}_3\text{SiH} \xrightarrow[\text{MeOH, H}_2\text{O}]{\text{KOH, 70°C}} {}^t\text{Bu}_3\text{SiOH} + \text{H}_2 \quad (9)$$

$$^t\text{Bu}_3\text{SiOH} + \text{Na} \xrightarrow[10\text{ h, }65\,^\circ\text{C}]{\text{hexanes}} (^t\text{Bu}_3\text{SiO})\text{Na} + 0.5\,\text{H}_2 \quad (10)$$

*Extreme caution* is necessary, because of the large quantities of $^t$BuLi required in typical preparations. Na(silox) is readily prepared (80–90%) as a colourless crystalline material via reflux of (silox)H with sodium in hexanes (eq. 10).

*Steric aspects of metathesis.* As in the preparation of tritox derivatives, metathetical reactions involving silox reagents provide a basis upon which an assessment of its steric influence can be made. Unlike the alkoxide, addition of Na(silox) to $ZrCl_4$ netted only the tris-silox complex, $(silox)_3ZrCl$ (**9**, 68%),[9] independent of the stoichiometry employed (eq. 11). Steric control was noted for addition of Na(silox) to $TiCl_4$, affording $(silox)_2TiCl_2$ (**10**)[16] or

$$\text{ZrCl}_4 + 3\,\text{Na(silox)} \xrightarrow[12\text{ h, }-3\,\text{NaCl}]{\text{THF, 25°C}} \underset{\mathbf{9}}{(\text{silox})_3\text{ZrCl}} \quad (11)$$

$$\text{TiCl}_4(\text{THF})_2 + 2\,\text{Na(silox)} \xrightarrow[12\text{ h, }-3\,\text{NaCl}]{\text{THF, 65°C}} \underset{\mathbf{11}}{(\text{silox})_3\text{TiCl}} \quad (12)$$

$(silox)_3TiCl$ (**11**, 85%, eq. 12)[9] depending on stoichiometry. Likewise, the synthesis of $(silox)_2MCl_3$ (M = Nb, **12**; Ta, **13**, eq. 13) and $(silox)_3MCl_2$ (M = Nb, **14**; Ta, **15**, m.p. 270°C, eq. 14) was readily accomplished via stoichiometric addition of Na(silox) to the appropriate pentachloride precursor.[13] In the original syntheses of **13** and **14** conducted by Weidenbruch,[17] $NbCl_5$ or $TaCl_5$ was heated in the presence of (silox)H, but the use of Na(silox) has led to improved yields (>70%).

$$\text{MCl}_5 + 2\,\text{Na(silox)} \xrightarrow[-2\,\text{NaCl}]{\text{tolune, }\Delta} \underset{\text{M = Nb, }\mathbf{12}\text{; Ta, }\mathbf{13}}{(\text{silox})_2\text{MCl}_3} \quad (13)$$

$$\text{MCl}_5 + 3\,\text{Na(silox)} \xrightarrow[-3\,\text{NaCl}]{\text{toluene, }\Delta} \underset{\text{M = Nb, }\mathbf{14}\text{; Ta, }\mathbf{15}}{(\text{silox})_3\text{MCl}_2} \quad (14)$$

While (tritox)H would not react with ($^t$Bu-$CH_2)_3Ta{=}CH{}^t$Bu, even when the two were melted together (>120°C), (silox)H/D cleaved a neopentyl group to yield (silox)($^t$Bu$CH_2)_2Ta{=}CH{}^t$Bu (**16**, 82%) upon thermolysis in toluene for 48 h at 75°C (eq. 15).[13] In contrast, silanolysis of $Zr(CH_2Ph)_4$

$$(^tBuCH_2)_3Ta{=}CH^tBu + (silox)Y \xrightarrow[75°C,\,48\,h]{toluene} (silox)(^tBuCH_2)_2Ta{=}CH^tBu + {}^tBuCH_2Y \quad (15)$$
$$Y = H, D \qquad\qquad \mathbf{16}$$

could not be controlled to prepare $(silox)Zr(CH_2Ph)_3$ cleanly (~90% purity); further reaction led to contamination with $(silox)_2Zr(CH_2Ph)_2$.[16]

The successful (and unsuccessful) stoichiometric metatheses involving silox reagents implicate a cone angle of >120°, yet less than that of tritox. Even though the Si—C bonds are 0.4 Å longer than corresponding C—C bonds of tritox, the greater Si—O bond length (~1.69 Å) relative to the C—O bond distance of tritox (~1.43 Å) apparently places the greater bulk of the $^tBu_3Si$ fragment further from the metal; consequently, the siloxide has a slightly smaller cone angle. The observations suggest that silox occupies a slightly greater degree of space than neopentyl, whose cone angle is estimated by Tolman to be 120°C.[4] $^1H$ NMR spectroscopic measurements are consistent with neopentyl and silox possessing relatively similar steric parameters.[13]

*Silox stability.* One need only refer to the original syntheses of early transition metal silox-halide and -oxo complexes by Weidenbruch[17] to appreciate the stability of these derivatives relative to tritox congeners. Through silanolyses of appropriate metal oxides, halides or oxyhalides, Weidenbruch isolated various species whose melting or decomposition points are a dramatic testament to the stability of the silox ligand: $[(silox)_2OV]_2(\mu-O)$, 271°C; $(silox)_2ClV{=}O$,[18] 177°C; $(silox)_3NbCl_2$ (**14**), 270°C; $(silox)_2MO_2$ (M = Cr, >200°C; Mo, 225°C, W), $(silox)ReO_3$, 245°C.

Silicon–oxygen bond strengths are estimated to be in the 130 kcal $mol^{-1}$ range,[19] substantially greater than the 90 kcal $mol^{-1}$ usually attributed to C—O single bonds. While care must be taken in using homolytic bond dissociation enthalpies to rationalize kinetic events, especially those implicated as possessing considerable heterolytic character, in this instance the correlation is obvious and probably relevant. Heterolytic C—O bond scission of a bound tritox is considered to occur via an $S_Ni$ type process (Scheme 1) to afford a transient $^tBu_3C^+$ cation,[12] but it is unlikely that a related process could occur for the silicon analogue. Instead, degradations involving nucleophilic attack at silicon are more rational, and these processes are undoubtedly hindered by the extreme bulk and electron-donating properties of the $^t$Bu groups.

*Crystallinity.* Virtually every pure silox derivative prepared in these laboratories crystallized readily. However, even small quantities of impurities can dramatically lower the melting point of certain compounds, because the intermolecular forces are effectively those of tert-butyl groups, which can be disrupted easily. All of the monomeric derivatives, and a large fraction of the dimeric complexes, are very soluble in hydrocarbon solvents. Both these factors contribute to difficulties in purification, unless the reaction occurs with >75% yields.

Structural studies constitute the most frustrating aspect of conducting silox chemistry. Data collection on silox derivatives has resulted in a success rate of only ~50%, where a passable solution is considered to be one with a reasonable solid state geometry and an $R < 12\%$. Disorder is almost always present in the $^t$Bu groups, and when it is particularly bad, a decent solution cannot be obtained, although the core of the molecule is rarely affected. Heavy atom problems have made structural investigation of bimetallic compounds a bad risk; disorder or ambiguity regarding the geometry of any bridging group is common.

*Bifunctional ligands*

As our program expanded, ligands possessing additional functionality were introduced in order to generate heterobimetallic complexes. Again, the basic principle of replacing or minimizing the use of Cp-type ligands was adhered to whenever possible in order to encourage the generation of reactive, electrophilic metal centres. We focused on alkoxyalkylphosphines because of their bridging capability in combining electrophilic, early transition metal centres with electron-rich, late metal fragments.

Thermolysis of $Ph_2PH$ and formaldehyde afforded $Ph_2PCH_2OH$ according to the method of Hellmann *et al.*[20,21] Variations of this ligand were produced via the ring opening of isobutylene oxide by $LiPPh_2$ (eq. 16)[22] or $LiCH_2PPh_2 \cdot TMEDA$ (eq. 17).[23] Another alkoxyalkylphosphine that proved

$$LiPPh_2 + Me_2\overline{CCH_2O} \xrightarrow[(2)\,H^+/H_2O/C_6H_6]{(1)\,THF} HOCMe_2CH_2PPh_2 \quad (16)$$

$$LiCH_2PPh_2 \cdot TMEDA + Me_2\overline{CCH_2O} \xrightarrow[(2)\,H^+/H_2O/C_6H_6]{(1)\,THF,\,-TMEDA} HOCMe_2CH_2CH_2PPh_2 \quad (17)$$

to be relatively useless was $HOC^tBu_2\,CH_2PPh_2$,[22] whose steric properties confined the ligand to behave as a chelate rather than a bridge. Conformational analysis was used to rationalize why

the phosphine linkages of $(Ph_2PCH_2C'Bu_2O)_2ZrX_2$ (X = Cl, **17**-Cl; Me, **17**-Me; $CH_2{}'Bu$, **17**-$CH_2{}'Bu$) and $(Ph_2PCH_2C'Bu_2O)_3ZrX$ (X = Cl, **18**-Cl; Me, **18**-Me) could not be successfully attached to late metals. In these cases, the increased steric bulk of the 'Bu groups proved to be a severe hindrance to bridge formation.

## HETEROBIMETALLIC CHEMISTRY

### *Introduction*

Heterogeneous catalysts responsible for the making and breaking of C—C, C—H and C—O bonds are typically comprised of electron-rich metals deposited on Lewis acidic, metal oxide supports. The role of the cocatalyst ranges from serving as a dispersive medium to one of extensive involvement. In the latter extremes, strong metal–support interactions (SMSI) of late metal/early metal oxide catalysts suggest that the components may function in a cooperative fashion. In these instances, the interface between metal oxide and late metal may determine the course of catalytic activity.

Various heterobimetallic complexes containing a "homogeneous interface" were synthesized and studied in order to model the interface of difunctional heterogeneous catalysts (Fig. 4). The heterodifunctional, bridging alkoxyalkylphosphine ligand was used to link the late metal (M′) and early metal (M) oxide centres. Hydrocarbon fragments coordinated to both an early and a late metal were investigated (e.g. framework A), and the character of early/late metal–metal bonds (e.g. framework B) was examined structurally and via molecular orbital calculations.

### *Alkyl exchange between* Pt *and* Zr

In order to probe a plausible migration of hydrocarbon fragments between disparate metal centres,

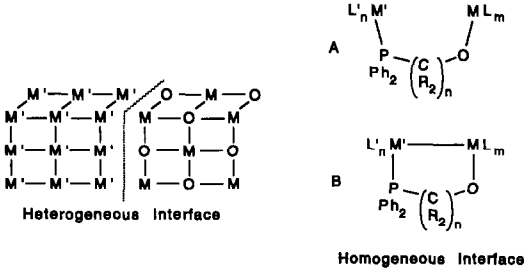


Fig. 4. The heterogeneous interface and its model homogeneous (with (B) or without (A) direct metal–metal interactions) interface; main group or early metal (MO or $ML_nO$-) electrophilic sites and late metal (M′ or $M'L'_nO$-) electron-rich sites.

a thermoneutral process involving the exchange of methyl groups between the Zr and Pt centres of $Cp^*MeZr(\mu\text{-}OCH_2Ph_2P)_2PtMe_2$ (**20**, Scheme 3) was investigated.[21] Kinetic studies of the approach to equilibrium of isotopomers such as **20**-Zr-$d_3$ and **20**-Pt-$d_3$ (eq. 18), monitored via $^1H$ and $^{195}Pt\{^1H\}$ NMR, were consistent with a first-order reaction.

$$\underset{\mathbf{20}-\mathrm{Zr}-d_3}{Cp^*(CD_3)Zr(\mu\text{-}OCH_2Ph_2P)_2Pt(CH_3)_2} \underset{k_{-1}}{\overset{2k_1}{\rightleftharpoons}} \underset{\mathbf{20}\text{-}\mathrm{Pt}-d_3}{Cp^*(CH_3)Zr(\mu\text{-}OCH_2Ph_2P)_2Pt(CH_3)(CD_3)} \quad (18)$$

However, the observation of an NMR isotope effect in the $^{195}Pt\{^1H\}$ NMR experiments indicated that all possible isotopomers were present, and that both uni- and bimolecular steps must therefore be considered. As a consequence, the equilibrium shown in eq. (18) was incorrect; in reality, a complex equilibrium was approached via the initial isotopomer, as eq. (19) illustrates. Through various kinetic experiments utilizing numerous isotopomers, accompanied by Runge–Kutta computer simula-

$$[\text{Zr-CD}_3] \underset{k'_{-1}}{\overset{2k'_1}{\rightleftharpoons}} [\text{Pt-CD}_3] \quad (19)$$

initially: $[\text{Zr-CD}_3] = [\mathbf{20}\text{-Zr-}d_3]$

at equilibrium:

$$[\text{Zr-CD}_3] = [\mathbf{20}\text{-Zr-}d_3] + [\mathbf{20}\text{-Zr-}d_3/\text{Pt-}d_3] + [\mathbf{20}\text{-}d_9]$$
$$[\text{Pt-CD}_3] = [\mathbf{20}\text{-Pt-}d_3] + [\mathbf{20}\text{-Zr-}d_3/\text{Pt-}d_3] + 2[\mathbf{20}\text{-Pt-}d_6] + 2[\mathbf{20}\text{-}d_9]$$

tions of each run, a mechanism incorporating slow unimolecular $CH_3/CD_3$ exchanges in combination with relatively fast bimolecular alkyl transfers was proposed. The enthalpy of activation [$\Delta H^{\ddagger} = 29.6(10)$ kcal mol$^{-1}$] suggested that phosphine loss could be playing the rate-determining role in mediation of the alkyl exchange, and the entropy of activation [$\Delta S^{\ddagger} = -5(3)$ eu] hinted that a Zr—Me group might be participating in an associative fashion.

Confirmation of the presence of alkyl exchange pathways between disparate metal centres was obtained in these experiments, and the results also reasserted the importance of redistribution reactions in organometallic chemistry. In addition, the homogeneous alkyl migration can be considered analogous to hydrogen spillover processes that are common to surfaces exhibiting SMSI.

### RhZr *heterobimetallic complexes*

*Bridging acyl formation.* Heterogeneous catalysts that exhibit the strong metal–support interaction

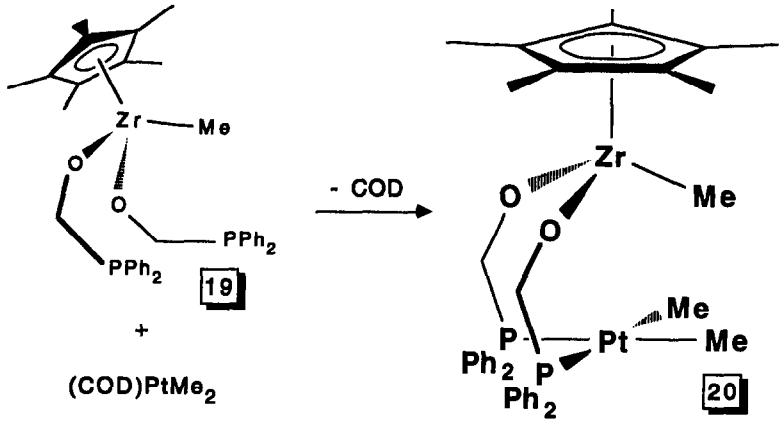


Scheme 3.

(SMSI) often produce oxygenates under Fischer–Tropsch conditions. In an effort to understand critical interactions of an oxygenated fragment at the interface between electrophilic and nucleophilic metal centres, a CO insertion reaction was chosen as a probe.[24]

As Scheme 4 illustrates, treatment of Cp*Zr(O-$CH_2PPh_2)_2$Me (**19**) with 0.5 equiv. $[(CO)_2RhCl]_2$ dimer affords a bridging acyl heterobimetallic complex, Cp*Zr($\mu$-$OCH_2PPh_2)_2$($\mu_2$-$\eta^2$-O=CMe)($\mu$-Cl)Rh(CO) (**21**). Cleavage of this oxygenated fragment was accomplished through the addition of electrophiles. Protonation with HCl afforded an intermediate $Rh^{III}$ $\mu$-acylhydride species, [Cp*Zr($\mu$-$OCH_2PPh_2)_2$($\mu_2$ - $\eta^2$ - O=CMe)($\mu$ - Cl)Rh(CO)H]Cl (**22**) before eliminating acetaldehyde to give Cp*Zr($\mu$-$OCH_2PPh_2)_2$($\mu$-$Cl_2$Rh(CO) (**23**). Alkylation of **21** with $CH_3I$ generated acetone and Cp*Zr($\mu$-$OCH_2PPh_2)_2$($\mu$-I)($\mu$-Cl)Rh(CO) (**24**), alternatively prepared from addition of NaI to **23**.

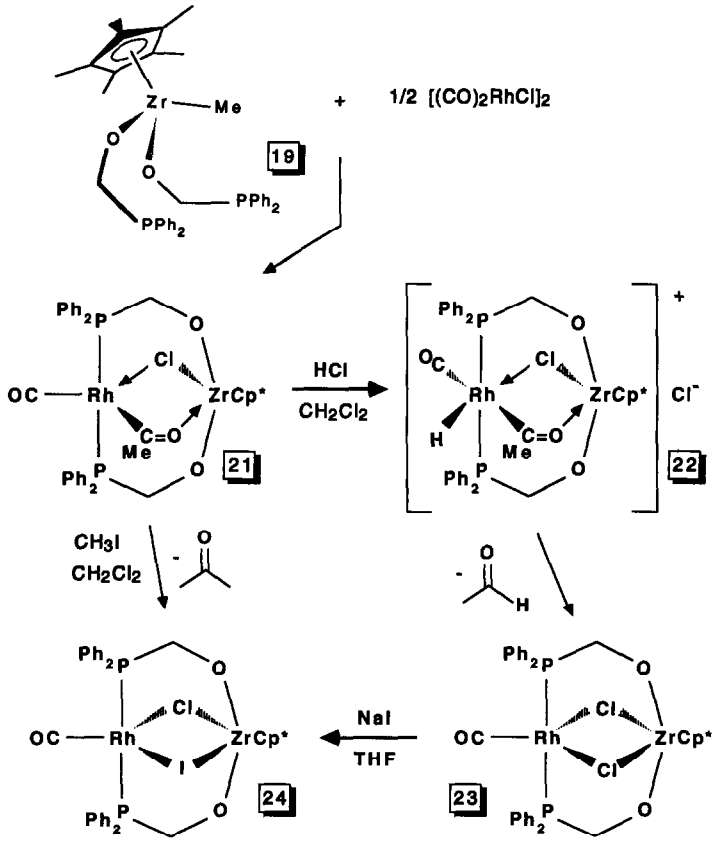


Scheme 4.

The formation of $Cp^*Zr(\mu\text{-}OCH_2PPh_2)_2(\mu_2\text{-}\eta^2\text{-}O{=}CMe)(\mu\text{-}Cl)Rh(CO)$ (**21**) occurs via a CO reduction sequence that utilizes both metals, since the $C_2$-oxygenate is comprised of a methyl derived from Zr and a CO from the rhodium. The 1490 $cm^{-1}$ absorption attributed to the $\mu$-acetyl CO stretch falls within the range of proposed surface acetates in heterogeneous systems. In stabilizing this fragment, both metals operate in a cooperative fashion; the more electron-rich Rh binds the $\mu$-acetyl through both $\sigma$- and $\pi$-bonding, while Zr functions as a strong oxophile. Protonation of **21** and the subsequent facile reductive elimination to acetaldehyde models the plausible product forming step in related heterogeneous processes.

Rh—Zr *metal–metal bonds*. For heterogeneous systems manifesting the characteristics of SMSI, the oxide support has often been reduced by some chemical process. As a consequence, it is conceivable that the metal–support interface contains discrete metal–metal bonds. In order to prepare complexes that would possess an M—M′ bond between the disparate metal centres, $Cp^*Zr(O CH_2Ph_2P)_2Me$ (**19**) was treated with $(Ph_3P)_3RhR$ (R = H, Me) in order to affect an addition of the Zr—Me bond across the Rh centre (Scheme 5).[24] For $(Ph_3P)_3RhMe$, this reaction occurred to afford $Cp^*Zr(\mu\text{-}OCH_2Ph_2P)_2RhMe_2$ (**25**), a complex resembling the earlier Zr/Pt dinuclear (**20**), except for the presence of an Rh—Zr bond. The X-ray crystal structure of **25** confirmed the presence of this linkage, whose bond length of 2.444 Å is ~0.25 Å shorter than the sum of Zr and Rh covalent radii. In accord with these data, molecular orbital calculations uncovered substantial $Rh(d\pi) \rightarrow Zr(d\pi)$ bonding, revealing a bond comprised of approximately 50% $\sigma$- and 50% $\pi$-character; thus the interaction is best considered as a double bond. When $(Ph_3P)_3RhH$ was the substrate, methane was eliminated from presumed intermediate $Cp^*Zr(\mu\text{-}OCH_2Ph_2P)_2RhMeH$ (**26**) to provide $Cp^*Zr(\mu\text{-}OCH_2Ph_2P)_2RhPPh_3$ (**27**).

The Rh—Zr bonded complexes exhibited extensive reaction chemistry, as illustrated in Scheme 6. Hydrogenation of $Cp^*Zr(\mu\text{-}OCH_2Ph_2P)_2RhMe_2$ (**25**) in the presence of $PPh_3$ afforded $Cp^*Zr(\mu\text{-}OCH_2Ph_2P)_2RhPPh_3$ (**27**), and further addition provided a dihydride, $Cp^*Zr(\mu\text{-}OCH_2Ph_2P)_2RhH_2PPh_3$ (**28**), a complex whose $PPh_3$ ligand was extremely labile (e.g. **29**) according to NMR spectroscopy. Heterobimetallic **28** catalysed the hydrogenation of ethylene as indicated, but this reaction was not explored further. Rh—Zr complex **27** added ethylene in forming $Cp^*Zr(\mu\text{-}OCH_2Ph_2P)_2Rh(C_2H_4)PPh_3$ (**30**), a compound that also manifested a labile phosphine (e.g. **31**) by $^{13}C\{^1H\}$ and $^{31}P$ NMR spectroscopy.

The preparation of these Rh—Zr metal–metal bonded complexes and their stability gives credence to the proposal that metal–support bonds are produced in bimetallic catalysts exhibiting SMSI. Questions regarding the type of reactivity occurring at this interface remain.

### *Heterobimetallics containing $\mu$-$CH_2$ and $\mu$-$CH_3$ fragments*

While it was relatively easy to generate Zr/Pt and Zr/Rh binuclears with Me groups on each metal centre, the synthesis of heterobimetallic complexes that contained hydrocarbon fragments bound to both metals proved more difficult. As mentioned previously, the construction of heterodinuclears was fraught with problems of ligand chelation and

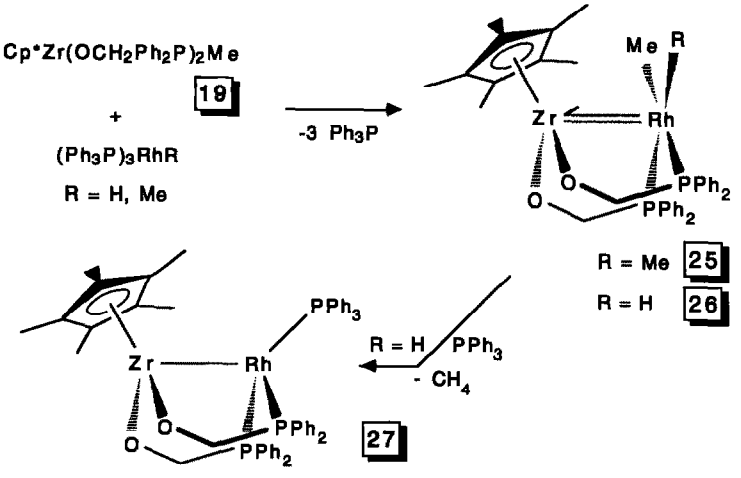


Scheme 5.

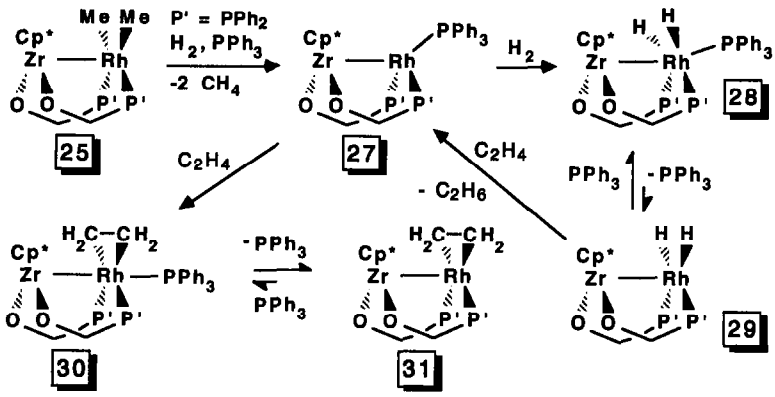


Scheme 6.

conformational constraints. Fortunately, the synthesis of $Me_3Ta(OCMe_2CH_2Ph_2P)_2$ (**32**) from $Me_3TaCl_2$ and $LiOCMe_2CH_2Ph_2P$ (eq. 20) rectified

$$Me_3TaCl_2 + 2LiOCMe_2CH_2Ph_2P \xrightarrow[-78^\circ C]{Et_2O} (Ph_2PCH_2CMe_2O)_2TaMe_3 + 2LiCl \quad (20)$$
**32**

many of these complications. Treatment ($C_7H_8$, 25°C) of **32** with $(COD)PtMe_2$ led initially to the precipitation of a colourless oligomer, [-$(Me)_3Ta(\mu$-$OCMe_2CH_2Ph_2P)Pt(Me)_2PPh_2CH_2CMe_2O$-]$_n$- (**33**), as shown in Scheme 7; subsequent thermolysis (THF, 100°C, 2–4 h) of **33** generated *trans*-$Me_2Ta(\mu$-$CH_2)(OCMe_2CH_2Ph_2P)_2PtMe$ (**34**) with concomitant methane. Scheme 8 illustrates an abbreviated, probable mechanism for the conversion of $(Ph_2PCH_2CMe_2O)_2TaMe_3$ (**32**) and $(TMEDA)NiMe_2$ to produce methane, ethane and $(TMEDA)Ta(\mu$-$CH_2)(\mu$-$Me)(\mu$-$OCMe_2CH_2Ph_2P)_2Ni$(**35**), a molecule that contains both $\mu$-$CH_2$ and $\mu$-$CH_3$ fragments. The latter unit exhibited an asymmetry in its $^1H$ NMR spectrum that revealed the expected Ta—$(H)_2$C—H—Ni bridging mode. A low barrier to equilibration of the bridging and terminal protons (i.e. $\Delta G^{\ddagger} \sim 8.8(2)$ kcal mol$^{-1}$, $T_c = -70$°C) was uncovered via variable temperature studies.

Bridging methylene and methyl groups are often postulated as heterogeneous surface intermediates in the Fischer–Tropsch reaction, hence these molecules are important models for the aforementioned bimetallic catalysts. However, the reactivity of the Ta/Pt and Ta/Ni heterobimetallic complexes proved to be disappointing. The former was relatively unreactive even at temperatures greater than 100°C,

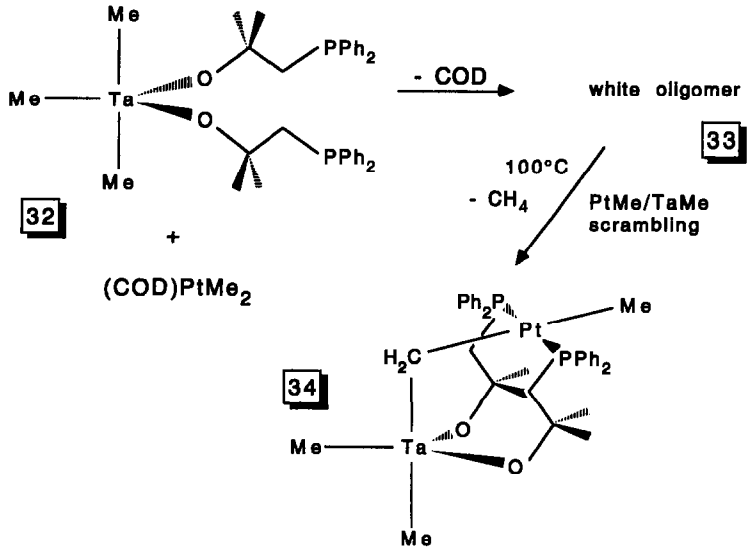


Scheme 7.

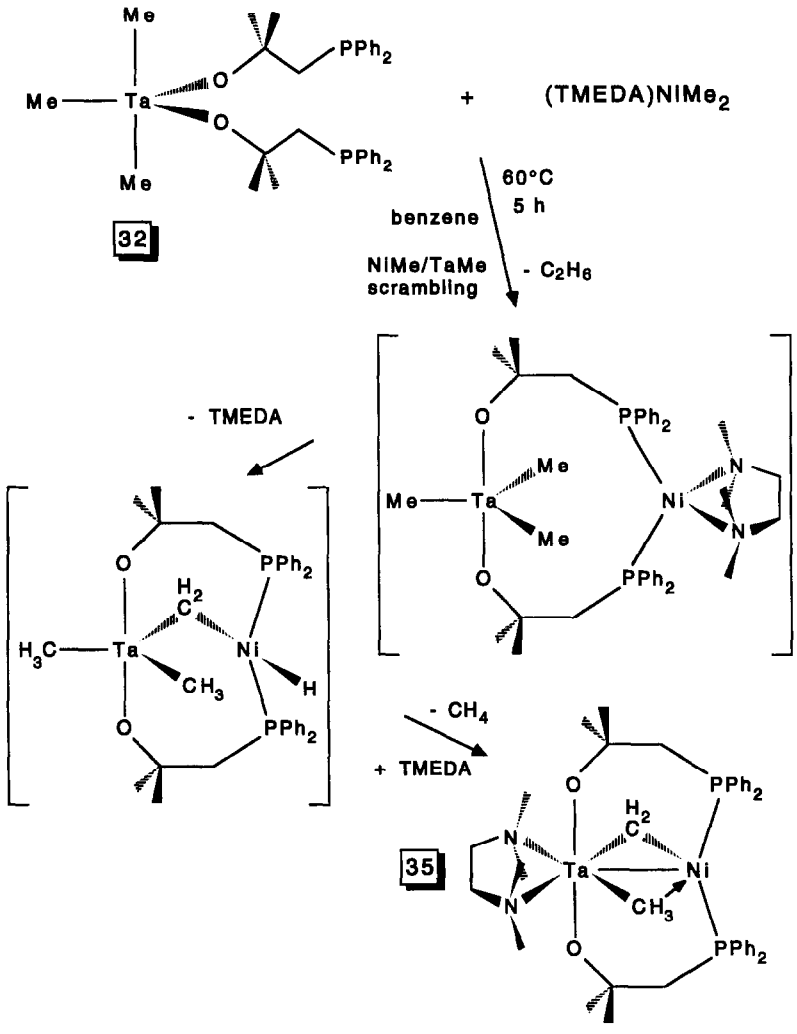


Scheme 8.

whereas the latter degraded swiftly under similar conditions. In probing the formation of the complexes by labelling studies [i.e. $(Ph_2PCH_2CMe_2O)_2Ta(CD_3)_3$ (**32**-$d_9$)], clear evidence for methyl exchange processes was obtained via mass spectra and $^{195}Pt\{^1H\}$ NMR spectroscopy, hence the amount of mechanistic information that could be obtained was limited.

## ELECTROPHILIC REACTIVITY OF HIGH OXIDATION STATE COMPLEXES

### *Dioxygen insertion and redistribution*

We rapidly discovered that group 4 tritox-alkyls possessed the electrophilic properties that were sought, because of their extreme dioxygen and water sensitivity. While the latter was clearly destructive, the former provided some intriguing chemistry. Exposure of $(tritox)_2MMe_2$ (M = Ti, **36**; Zr, **37**; Hf, **38**) to dry dioxygen afforded the corresponding dimethoxide derivatives, $(tritox)_2M(OMe)_2$ (M = Ti, **39**; Zr, **40**; Hf, **41**) in ~90% yield (eq. 21), independent of solvent (hexane, $C_6H_6$, toluene, $CH_2Cl_2$, $CCl_4$, $Et_2O$).[25] The zir-

$$(tritox)_2MMe_2 + O_2 \xrightarrow{\text{hexanes}} \underset{\text{M = Ti, 39; Zr, 40; Hf, 41}}{(tritox)_2M(OMe)_2} \quad (21)$$

M = Ti, **36**; Zr, **37**; Hf, **38**

conium and hafnium derivatives were converted immediately at −78°C, while the titanium dimethyl required extended, irregular reaction times (8–30 h) depending on the batch used, even though each was spectroscopically identical. Addition of $O_2$ to $(tritox)TiMe_3$ (**42**) generated $(tritox)TiMe_{3-x}(OMe)_x$ ($x$ = 1, **43**, 95%; 2, **44**, 84%; 3, **45**, 74%), depend-

ing on the stoichiometry (eq. 22). Curiously, (tritox)

$$\underset{\mathbf{42}}{\text{(tritox)TiMe}_3} + x/2\,O_2 \longrightarrow \underset{x = 1, \mathbf{43}; 2, \mathbf{44}; 3, \mathbf{45}}{\text{(tritox)TiMe}_{3-x}(OMe)_x} \quad (22)$$

$TiMe_2(OMe)$ (**43**) was practically colourless—as were the other methoxides—but there was a faint yellow tint to its solutions, and crystals of the complex were orange; structural studies showed **43** to be a dimer of $C_{2h}$ symmetry in the solid state, consisting of two square pyramidal units linked by basal $\mu$-$OCH_3$ bridges that lie on the two-fold axis (Fig. 5). The orange colour is attributed to a lowering of $O(p\pi) \rightarrow Ti(d\pi)$ LMCT transitions due to weak $Ti(d\pi) \cdots Ti(d\pi)$ overlap in the dimer. Molecular weight measurements indicated that **43** manifested a monomer/dimer equilibrium in benzene solution.

Exchange of methoxide ligands was rapid among the complexes above. Solutions initially containing $(tritox)_2ZrMe_2$ (**37**) and $(tritox)_2Hf(OMe)_2$ (**41**) rapidly equilibrated with $(tritox)_2HfMe_2$ (**38**) and $(tritox)_2Zr(OMe)_2$ (**40**); $K_{eq} \sim 1$ (eq. 23). No methoxy–methyl intermediates were detected. Like-

$$\underset{\mathbf{37}}{(tritox)_2ZrMe_2} + \underset{\mathbf{41}}{(tritox)_2Hf(OMe)_2} \rightleftharpoons \underset{\mathbf{38}}{(tritox)_2HfMe_2} + \underset{\mathbf{40}}{(tritox)_2Zr(OMe)_2} \quad (23)$$

wise, the combination of (tritox)$TiMe_3$ (**42**) and (tritox)$TiMe(OMe)_2$ (**44**) converted completely to (tritox)$TiMe_2(OMe)$ (**43**) at 25°C (eq. 24); (tritox)

$$\underset{\mathbf{42}}{\text{(tritox)TiMe}_3} + \underset{\mathbf{44}}{\text{(tritox)TiMe(OMe)}_2} \rightleftharpoons 2\underset{\mathbf{43}}{\text{(tritox)TiMe}_2\text{(OMe)}} \quad (24)$$

$$\underset{\mathbf{45}}{\text{(tritox)Ti(OMe)}_3} + \underset{\mathbf{43}}{\text{(tritox)TiMe}_2\text{(OMe)}} \rightleftharpoons 2\underset{\mathbf{44}}{\text{(tritox)TiMe(OMe)}_2} \quad (25)$$

$TiMe_2(OMe)$ (**43**) and (tritox)$Ti(OMe)_3$ (**45**) reapportioned to give solely (tritox)$TiMe(OMe)_2$ (**44**) according to $^1H$ NMR spectroscopic monitoring (eq. 25). It is likely that these redistribution reactions are critical to the mechanism and product distributions of the oxygenations of **42**. It is noteworthy that complications from redistribution of the tritox ligands were not observed in any of the oxygenation and exchange studies.

### *Autoxidation and oxygen atom transfer*

Although the mechanism(s) of the metal–alkyl oxygenations above appeared to involve an alkylperoxy intermediate, as indicated in Scheme 9, substantive support for an MOOR intermediate was lacking, and the nature of the $O_2$ insertion reaction was unknown. If the coordination sphere of a metal alkylperoxide contained an allylic alkoxide, epoxide formation was expected to occur via oxygen atom transfer, just as in the titanium tetraisopropoxide-based Sharpless epoxidation reactions. Through metathetical procedures, $(tritox)_2ZrMe$

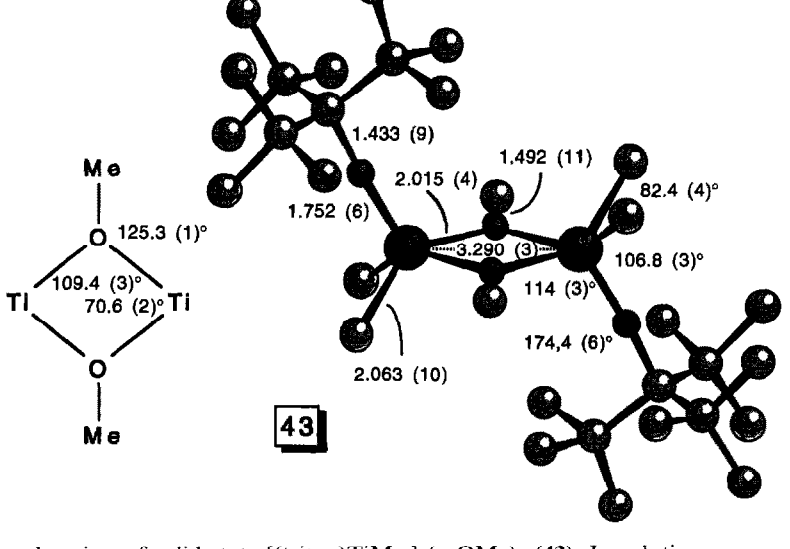


Fig. 5. Molecular view of solid state $[(tritox)TiMe_2]_2(\mu\text{-}OMe)_2$ (**43**). In solution, a monomer/dimer equilibrium exists.

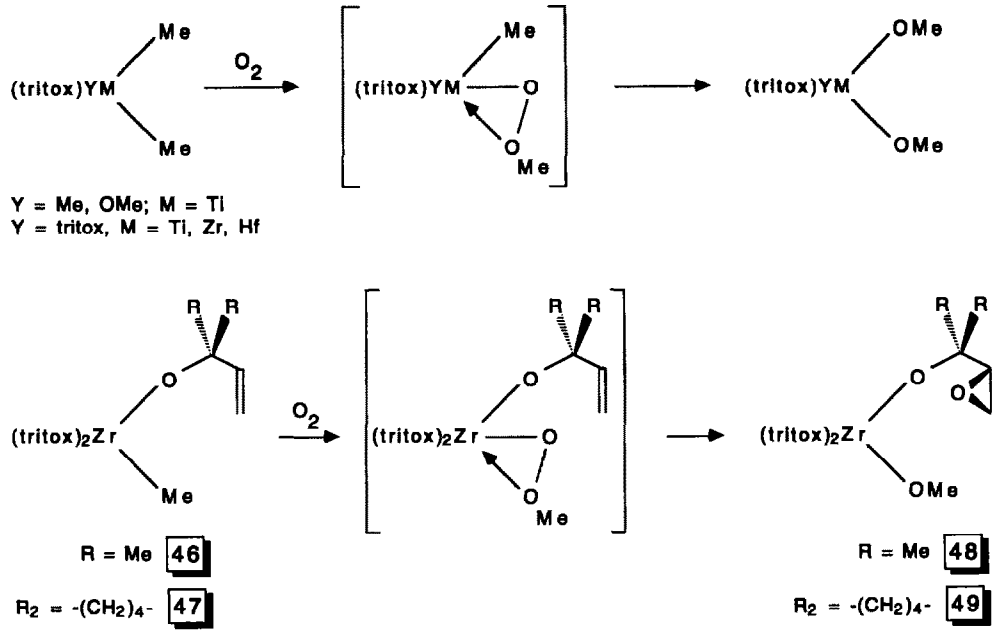


Scheme 9.

($OCR_2CH{=}CH_2$) [R = Me, **46**; $R_2$ = —$(CH_2)_4$—, **47**] derivatives were prepared and exposed to $O_2$, yielding the epoxide derivatives, (tritox)$_2$Zr(OMe)($OCR_2\overline{CHCH_2O}$) [R = Me, **48**; $R_2$ = —$(CH_2)_4$—, **49**].[25] As Scheme 9 indicates, methylperoxide intermediates are thought to mediate the oxygen-atom transfer.

While this result provided crucial evidence favoring alkylperoxide intermediates, the mechanism of the overall oxygenation process, specifically the $O_2$ insertion step, was unknown. Crossover experiments with **47** and $CD_3$-labelled **46** revealed that the methyl groups of each starting material ended up in the methoxide of both products, i.e. crossover occurred. Additional experiments were consistent with the radical chain processes shown in Scheme 10, although the nature of the initiation event is ambiguous. Briefly, dioxygen initiates some Zr—Me bond cleavage and generates methyl radical (or an initiator induces the generation of Me·), which scavenges $O_2$ at diffusion controlled rates—rates that are competitive with Cl· abstraction from halogenated solvents—to produce methylperoxy radical in the first propagation step. In the ensuing propagation step, $MeO_2$· attacks a zirconium centre, regenerating methyl radical and forming the methylperoxide intermediate. Subsequent O-atom transfer affords the epoxide product. Standard termination events, such as radical coupling reactions, are suspected but supporting evidence was not obtained.

It was reassuring to note the parallels between group 4 oxygenation and redistribution reactions and those of the main group alkyls (e.g. $BR_3$, $AlR_3$ etc.), for which autoxidation processes were well documented. Features common to both types of metals include electronic (i.e. coordinative) unsaturation, and metal–alkyl bonds that are polarized, $M^{\delta+}$—$R^{\delta-}$. Such characteristics also describe metal surfaces, hence the oxidation of surface alkyl species may proceed via related autoxidation pathways. The epoxidation sequence also complements the mechanistic underpinning of Sharpless' Ti-catalysed epoxidation procedures, while clearly showing that dioxygen is not necessarily an anathema to organometallic systems!

*Nitride clusters*

Polyoxo- and heteropolyoxo anions comprise a common class of cage and cluster compounds, yet until recently nitrogen-based analogues were virtually non-existent. Eschewing solid state methods of synthesis, we viewed the preparation of N-based clusters as occurring via ammonolyses of early transition metal alkyl complexes.[26] A directing group on the metal—in our case, the bulky alkoxide tritox—would encourage cluster generation relative to the usual alternative: the formation of amorphous oligomers.

As Scheme 11 reveals, ammonolysis of (tritox)Zr($CH_2Ph$)$_3$ (**5**) enabled the preparation of three cage compounds.[27] Treatment of **5** with 1.0 equiv. of $NH_3$ in benzene for ~5 days at 25°C provided colourless crystals of a ~0.6 : 1.0 composite of pseudo-octahedral, $C_2$ [(tritox)Zr]$_6$($\mu_6$-N)

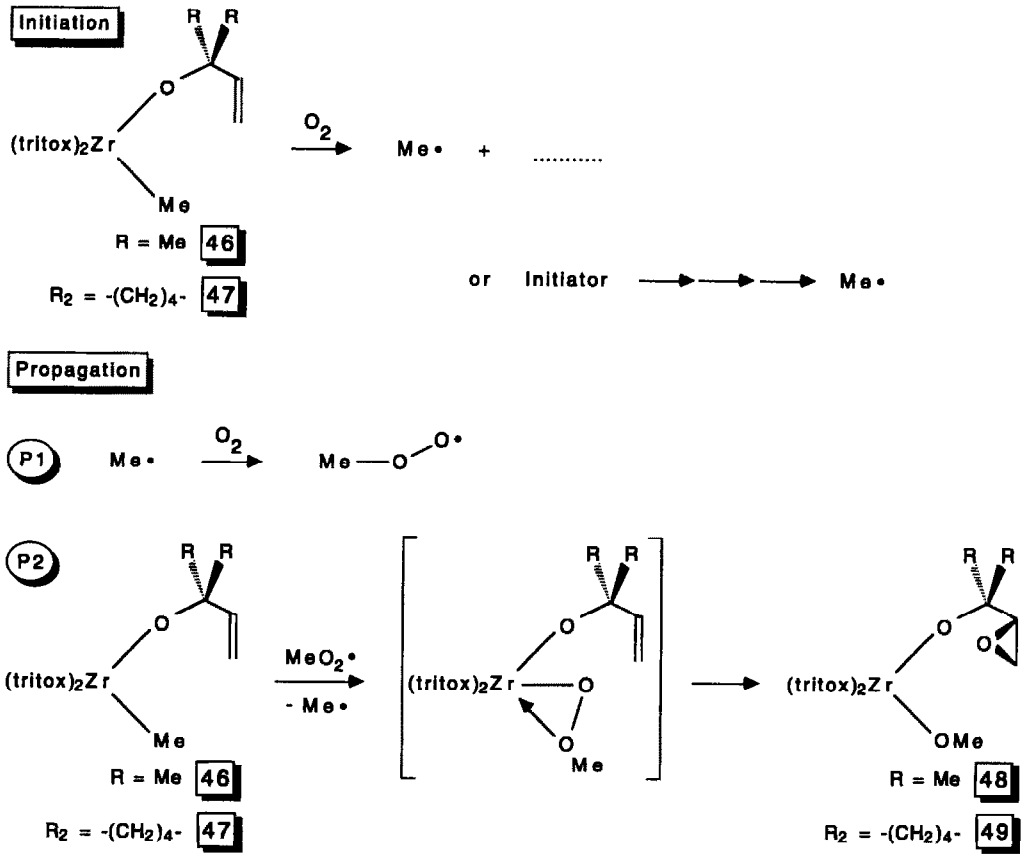


Scheme 10.

$(\mu_3\text{-NH})_6(\mu_2\text{-NH}_2)_3$ (**50**) and square pyramidal $[(\text{tritox})\text{Zr}]_5(\mu_5\text{-N})(\mu_3\text{-NH})_4(\mu_2\text{-NH}_2)_4$ (**51**) according to crystallographic and CPMAS NMR investigations. Addition of 1.75 equiv. of $NH_3$ to benzene solutions of **5** at 25°C generated pure, colourless crystals of **51** (32%), whose structure was confirmed by X-ray crystallography. Exposure of **5** to 2.6 equiv. of $NH_3$ or treatment of **51** with excess ammonia produced the dodecaamido cluster, $[(\text{tritox})\text{Zr}]_5(\mu_5\text{-N})(\mu_2\text{-NH}_2)_{12}$ (**52**). In solution, **52** was observed in equilibrium with **51** and 4.0 equiv. of $NH_3$.

The cluster cores are related to simple cubic lattices, and the $^{15}N$ NMR shifts of the $\mu$-$N_6$ (**50**, $\delta$ −40.6) and $\mu$-$N_5$ (**51**, $\delta$ −62.6; **52**, $\delta$ −6.5) ligands are comparable to that of cubic ZrN (CPMAS $^{15}N$ NMR: $\delta$ −20). Note that the electrophilic character of the $(\text{tritox})\text{Zr}^{3+}$ core encourages coordination of five additional nitrogen donors in the cases of **50** and **51**, while NMR spectral evidence supports a higher coordination number for the zirconium in the dodecaamide **52**.

While we managed to prepare nitrogen-based polyoxoanion analogues containing nitride ($N^{3-}$), imide ($NH^{2-}$) and amide ($NH_2^-$) ligands, these methods have not proven to be general, and much work needs to be done to expand the scope of this class of molecules.

## LOW-VALENT COMPLEXES

### *Introduction*

The most interesting feature of the silox ligand is its ability to stabilize reduced early transition metal centres. Perhaps the most pertinent spectroscopic information about this property of the ligand is provided by the XPS spectra of $(\text{silox})_2\text{TiCl}_2$ (**10**)[16] and $(\text{silox})_3\text{TiCl}$ (**11**),[9] taken by Prof. Frank Feher and his colleagues at Univ. California, Irvine.[28] The data are compared to those of $Cp_2TiCl_2$ and $Cp^*_2TiCl_2$ in Table 1. From electrochemical and XPS studies, Gassman *et al.* concluded that the substitution of two Cp ligands by two Cp* groups has an electronic effect approaching a one-electron reduction, since a 0.8 eV difference in binding energy (BE) was typically observed.[29] Inspection of the data in Table 1 reveals that although both $Cp_2TiCl_2$ and $(\text{silox})_2\text{TiCl}_2$ are formally considered $Ti^{IV}$ species, the $\text{Ti}(2p_{3/2})$ binding energies show that

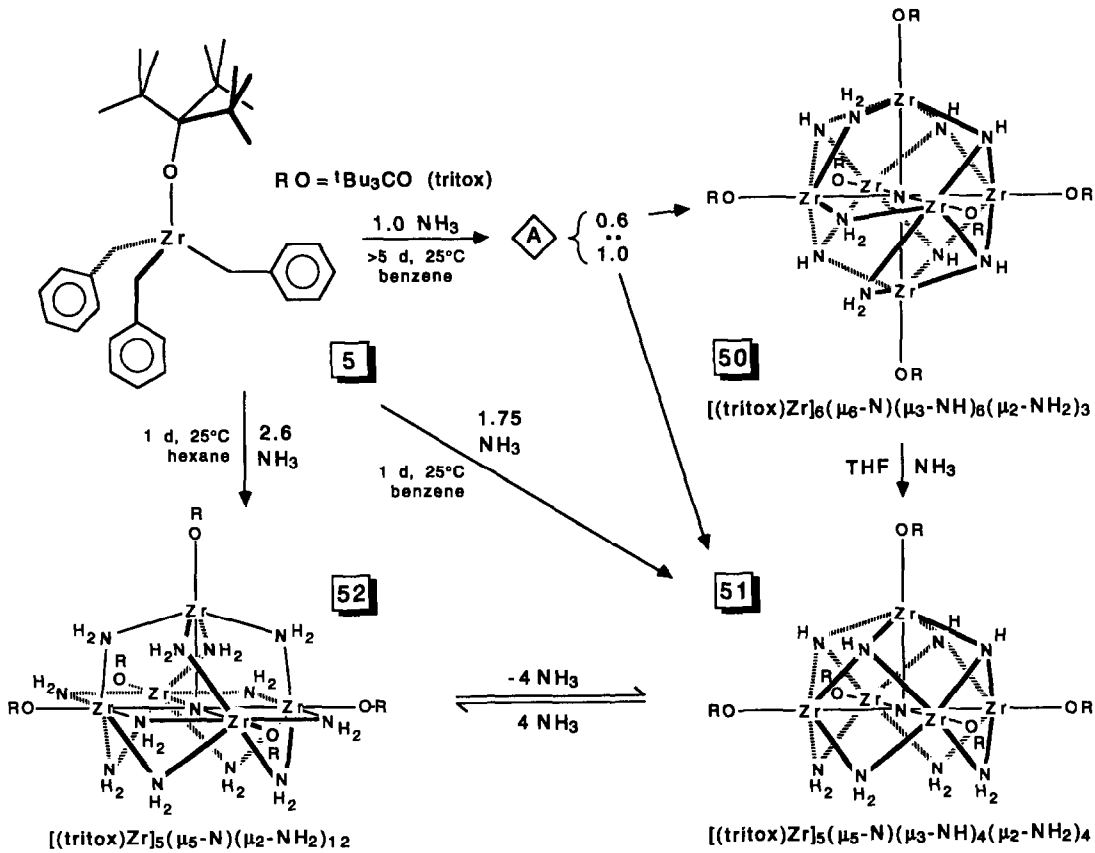


Scheme 11.

Table 1. Ti XPS data (eV) for silox and Cp/Cp* titanium complexes[a]

| | $(silox)_3TiCl$ | $(silox)_2TiCl_2$ | $Cp_2TiCl_2$ | $Cp^*_2TiCl_2$ |
|---|---|---|---|---|
| $Ti(2p_{1/2})$ | 465.00 | 464.40 | 463.35(463.0) | (462.2) |
| $Ti(2p_{3/2})$ | 459.20 | 458.70 | 457.45(456.9) | (456.1) |

[a] Data are from Ref. 28; data in parentheses are from Ref. 29. All spectra internally referenced to carbon (284.60 eV). The $Ti(2p_{3/2})$ shows a lower binding energy and is 2–3 times more intense than $Ti(2p_{1/2})$.

the silox derivative is 1.25 eV more difficult to ionize. Substitution of chloride by another silox results in another increase of 0.50 eV in $Ti(2p_{3/2})$ binding energy. According to the XPS data, silox renders a metal centre approximately 0.5 eV more electrophilic than either chloride or Cp, presumably due to the electronegativity of oxygen, combined with its diminished capacity for $O(p\pi) \rightarrow Ti(d\pi)$ donation due to purported $O(p\pi) \rightarrow Si(d\pi)$ interactions.

The XPS data provide a rationale for the unexpected stability of low-valent silox derivatives. It can be inferred that $(silox)_3Ti$ (**53**) should have a BE similar to that of $Cp_2TiCl_2$.[9] Provided the binding energies also reflect the thermodynamic stability of a compound, it is clear the silox is compatible with a reduced metal centre that remains very electrophilic. This combination of potent reduction potential and electrophilicity is responsible for the unusual reactivity evident in low-valent silox derivatives.

## $(silox)_3Ti$

*Synthesis.* Reduction of $(silox)_3TiCl$ (**11**) with Na/Hg in DME produced a light-green, $Ti^{III}$ DME adduct, $(silox)_3Ti(DME)$ (**53**-DME, eq. 26); removal of the DME in toluene provided orange

(silox)$_3$Ti (**53**) in 76% yield (eq. 27) after crystal-

$$\underset{\mathbf{11}}{(\text{silox})_3\text{TiCl}} \xrightarrow[\text{DME}]{\text{Na/Hg, -NaCl}} \underset{\mathbf{53}\text{-DME}}{(\text{silox})_3\text{Ti(DME)}} \quad (26)$$

$$\mathbf{53}\text{-DME} \xrightarrow{\text{toluene}} \underset{\mathbf{53}}{(\text{silox})_3\text{Ti}} + \text{DME} \quad (27)$$

lization from hexanes.[9] The use of DME was crucial because **53** reacted with other ethereal solvents such as THF and $Et_2O$.

*Spectroscopy.* The UV–vis spectrum of monomeric, pseudo-$D_{3h}$ (silox)$_3$Ti (**53**) consisted of the $^2A' \rightarrow {}^2E'$ [$(d_{z^2})^1 \rightarrow (d_{x^2-y^2}, d_{xy})^1$) transition at 500 nm ($\varepsilon$ = 360 $M^{-1}$ $cm^{-1}$) and two intense absorptions at 248 nm ($\varepsilon$ = 13,600 $M^{-1}$ $cm^{-1}$) and 211 nm ($\varepsilon$ = 15,000 $M^{-1}$ $cm^{-1}$), assigned as LMCT and intraligand in character, respectively. No electronic transitions were identified in the near-infrared region. From spectral comparisons to related three-coordinate $Ti^{III}$ derivatives, the ligand field strength of silox should be considered near or perhaps slightly stronger than 2,6-$^t$Bu-$C_6H_3O$, and significantly stronger than $(Me_3Si)_2N$.

The 25°C EPR spectrum of **53** manifested a single absorption with an isotropic $g_{iso}$ = 1.9554, and hyperfine couplings to $^{47}$Ti ($S$ = 5/2, 7.5%) and $^{49}$Ti ($S$ = 7/2, 5.5%) of $a_{iso}$ = 155 MHz (~56.7 G). The powder spectrum of **53** in toluene at 77 K exhibited axial symmetry, with $g_{||}$ = 1.9997 and $g_{\perp}$ = 1.9323, accompanied by hyperfine couplings of $a_{||}$ = 171 MHz (~61.2 G) and $a_{\perp}$ ~ 153 MHz (~56.8 G), respectively. The large hyperfine splittings are consistent with a singly occupied $d_{z^2}$ orbital, since extensive mixing with the 4$s$ orbital is predicted in $D_{3h}$ or lower symmetry.[9]

*Ketyl formation by* (silox)$_3$Ti. A critical, but unseen, intermediate in the pinacol and related transition metal-mediated reactions is a ketyl species. Numerous donor-adducts of (silox)$_3$Ti (**53**), characterized via UV–vis and EPR spectra, have been prepared, including ink-blue ketyl complexes, (silox)$_3$TiOCRR′· (**53**-OCRR′: R, R′ = Ph, $p$-Me-Ph, $^t$Bu; R = $^t$Bu, R′ = H; R = $^t$Bu, R′ = Me; O=CRR′ = 3,3,5,5-Me$_4$-cyclohexanone), that form upon exposure to various bulky organic carbonyls (eq. 28). Kctyls **54**-OCRR′ possessed EPR spectra consistent with transposition of the electron from

$$\underset{\mathbf{53}}{(\text{silox})_3\text{Ti}} + \text{O=CRR}' \xrightarrow{\text{toluene}} \underset{\mathbf{54}\text{-OCRR}'\cdot}{(\text{silox})_3\text{TiOCRR}'\cdot} \quad (28)$$

Ti to the carbonyl carbon as exemplified by spectra of the benzophenone adduct (**54**-OCPh$_2$·) illustrated in Fig. 6. As Scheme 12 reveals, **54**-OCPh$_2$· was found to be in equilibrium with [(silox)$_3$TiOCPh$_2$]$_2$ (**55**; $K_{eq}$(25°C) = [**54**-OCPh$_2$·]$^2$/[**55**] = $7.5 \times 10^{-7}$ M, $\Delta H_{diss}$ = 18(1) kcal mol$^{-1}$, $\Delta S_{diss}$ = 33(3) eu), a dimer exhibiting a C—C bond between a carbonyl carbon and the *para* position of a phenyl, akin to hexaphenylethane. Exposure of the **54**-OCPh$_2$·/**55** mixture to Ph$_3$SnH afforded the diphenylmethoxide derivative, (silox)$_3$TiOCHPh$_2$ (**56**), via H-atom transfer. When small ketones with α-hydrogens are exposed to **53**, disproportionation reactions ensue. Acetone reacted with **53** to give the isopropoxide and 2-propenoxide species, (silox)$_3$Ti(OCHMe$_2$) (**57**) and (silox)$_3$Ti(OMeC=CH$_2$) (**58**), respectively, following hydrogen atom transfer between two acetone ketyl complexes, (silox)$_3$Ti(OCMe$_2$·) (**54**-OCMe$_2$·, eqs 29, 30).

$$\underset{\mathbf{53}}{(\text{silox})_3\text{Ti}} + (\text{H}_3\text{C})_2\text{C=O} \xrightarrow{\text{hexanes}} \underset{\mathbf{54}\text{-OCMe}_3\cdot}{(\text{silox})_3\text{Ti-OCMe}_2\cdot} \quad (29)$$

$$2\,\mathbf{54}\text{-OCMe}_2\cdot \xrightarrow{\text{hexanes}} \underset{\mathbf{57}}{(\text{silox})_3\text{Ti(OCHMe}_2)} + \underset{\mathbf{58}}{(\text{silox})_3\text{Ti(OMeC=CH}_2)} \quad (30)$$

(silox)$_3$Ta

*Synthesis.* By far the most interesting low-valent complex that we have investigated is (silox)$_3$Ta (**59**), prepared via Na/Hg reduction of (silox)$_3$TiCl$_2$ (**15**) in 74% yield (eq. 31).[30] Cryoscopic molecular weight measurements were consistent with a mono-

$$\underset{\mathbf{15}}{(\text{silox})_3\text{TaCl}_2} \xrightarrow[\text{THF, 25°C, 2 h}]{\text{Na/Hg, -2NaCl}} \underset{\mathbf{59}}{(\text{silox})_3\text{Ta}} \quad (31)$$

mer, and various NMR spectra in conjunction with magnetic susceptibility measurements showed that **59** possesses a singlet ground state ($^1A_1'$ in $D_{3h}$) from 2 to 300 K. It is exceedingly rare to find a three-coordinate, low-valent, third row derivative of the early metals, given the propensity of these metals to form high-valent, high-coordinate complexes. As discussed above for (silox)$_3$Ti (**53**), it is clear that the silox ligand possesses a unique ability to stabilize reduced metal centres.

*UV–vis spectroscopy.* The UV–vis spectrum of $D_{3h}$ (silox)$_3$Ta (**59**) provides some insight into its character and hence its unusual coordination geometry.[31] The $d^2$ species exhibits a rather complex spectrum dominated by intraligand (1L) and ligand-to-metal charge transfer (LMCT) bands at

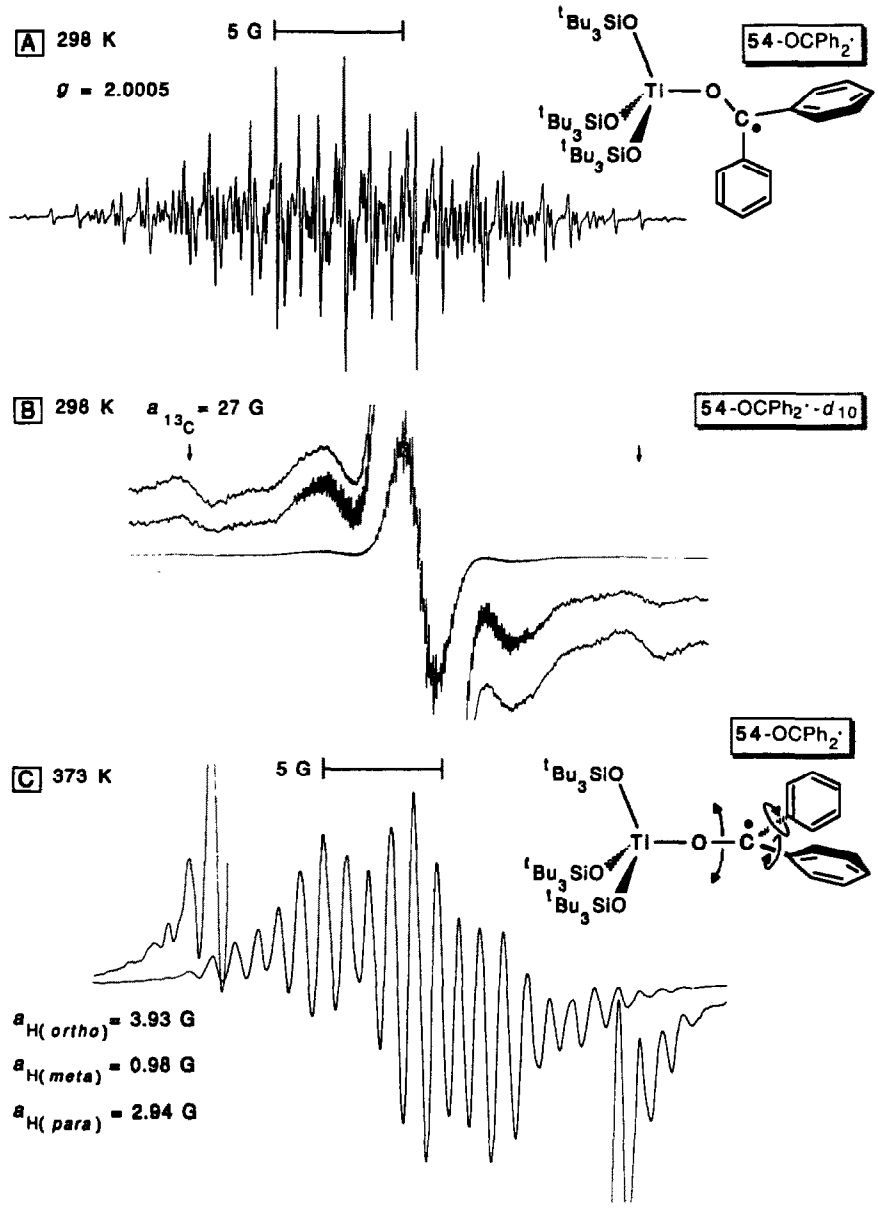


Fig. 6. (A) EPR spectrum (toluene) of (silox)$_3$Ti(OCPh$_2$·) (**54**-OCPh$_2$·) showing >125 lines indicative of inequivalent Ph rings, hindered ring rotation, or both. (B) Compressed EPR spectrum (toluene) of **54**-OCPh$_2$·-$d_{10}$ revealing a lack of notable Ti hyperfine lines ($a_{Ti}$ < 2 G), a residual proton coupling, and a $^{13}$C splitting. (C) EPR spectrum (toluene) of **54**-OCPh$_2$· at 100°C, exhibiting 27 lines as ring equilibration is nearly complete.

216 ($\varepsilon \sim 6800\ cm^{-1}\ M^{-1}$) and 306 nm ($\varepsilon \sim 13{,}000$), respectively. Its blue colour originates from a transmission window near 480 nm, while its pale appearance is due to the weak character ($\varepsilon = 36\ cm^{-1}\ M^{-1}$) of the only absorption in the visible region, centred at 612 nm. Two subtle shoulders on this band are also evident at ~570 ($\varepsilon \leqslant 5\ cm^{-1}\ M^{-1}$) and ~695 nm ($\varepsilon \sim 25\ cm^{-1}\ M^{-1}$). In the near-IR, a broad absorption is centred at 928 nm ($\varepsilon = 34\ cm^{-1}\ M^{-1}$) with an accompanying shoulder at 840 ($\varepsilon \sim 25\ cm^{-1}\ M^{-1}$). These broad, weak bands are tentatively assigned as triplet absorptions arising from the $a_1'^2 \rightarrow a_1'^1\ e''^1$ transition. Rigorously, only one triplet ($^1A_1' \rightarrow {}^3E''$) results from this electron configuration; however, any distortion from $D_{3h}$ symmetry will split the $e''$ $\pi$-type orbitals, resulting in two bands. The large energy difference between the two bands argues against splitting due to a spin–orbit coupling, but the shoulders accompanying each absorption may reflect these interactions.

Several bands not obscured by the IL and LMCT absorptions appear in the near-UV at 238 ($\varepsilon \sim 2000$

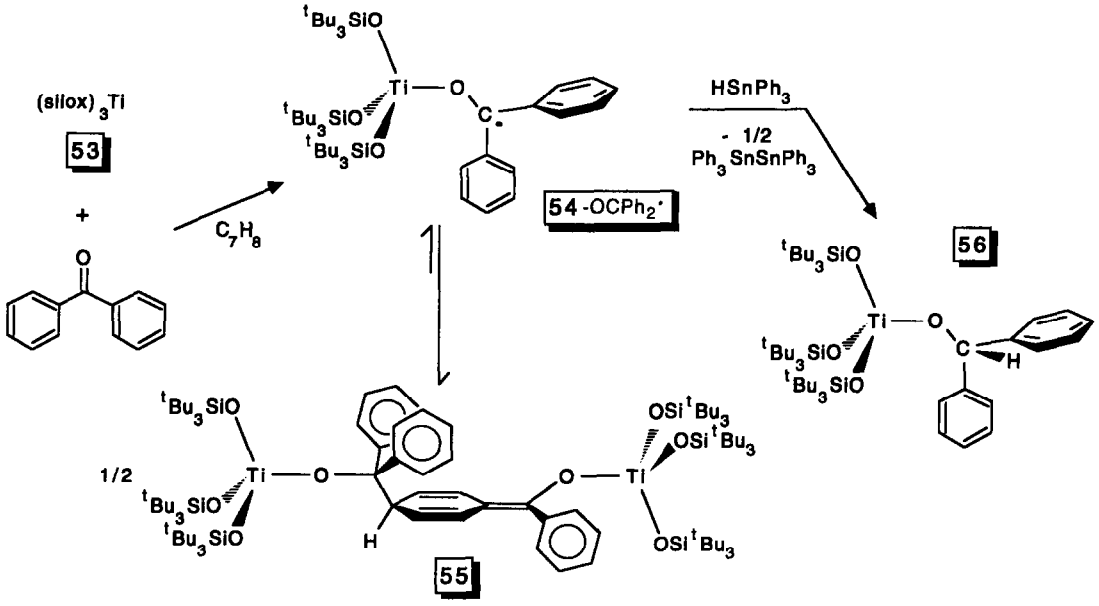


Scheme 12.

$cm^{-1}$ $M^{-1}$), 350 ($\varepsilon \sim 1000$ $cm^{-1}$ $M^{-1}$), 364 ($\varepsilon \sim 2400$ $cm^{-1}$ $M^{-1}$) and 394 nm ($\varepsilon \sim 1100$ $cm^{-1}$ $M^{-1}$), each possessing similar extinction coefficients. The 238 nm band is assigned as the *xy*-allowed $^1A_1' \rightarrow {}^1E'$ ($a_1'^2 \rightarrow a_1'^1 e'^1$) transition, since it appears at nearly twice the energy of the corresponding band in the related $d^1$ (silox)$_3$Ti (**53**) complex, as expected for a third row species. The 364 nm band is assigned as the electric dipole forbidden $^1A_1' \rightarrow {}^1E''$ ($a_1'^2 \rightarrow a_1'^1 e''^1$) transition, presumably strong due to intensity stealing from the charge transfer absorptions, vibronic coupling and the breakdown from rigorous $D_{3h}$ symmetry. One of the neighbouring bands could also result from slight splitting of the $e''$ orbitals.

From the convention of Wood,[32] and the above assignments, the orbital energies may be estimated as: $a_1'$ ($d_{z^2}$), $-29{,}500$ $cm^{-1}$; $e''$ ($d_{xz}$, $d_{yz}$), $-2040$; $e'$ ($d_{xy}$, $d_{x^2-y^2}$), 16,800. The resulting CFSE of $-59{,}000$ $cm^{-1}$ reveals that the silox groups impart a very strong ligand field about (silox)$_3$Ta (**59**). Two other features of the *d*-orbital energetics warrant attention. First, the $d_{z^2}$ orbital is extremely low in energy, indicative of minimal $\sigma^*$ character, thus the *d*-electron density is located above and below the $TaO_3$ plane. Second, the relative energy of the $e''$ set is extremely high, supporting the contention that silox is an effective $\pi$-donor, despite the Si substituent.

*$\eta^2$-Pyridine and related adducts.* While oxidative addition reactions of (silox)$_3$Ta (**59**) were expected to be interesting, some intriguing surprises were observed in examining simple adduct formation.[31,33] Although (silox)$_3$Ta (**59**) is stable in solution for periods of hours, in concentrated benzene solutions, brown crystals of a benzene adduct [(silox)$_3$Ta]$_2$ ($\mu$-$C_6H_6$) (**60**) formed in meagre yield (~7%). Figure 7 illustrates a model of the disordered core of this strange bridging benzene complex, and shows that prolonged dissolution of **59** eventually results in cyclometallation to give (silox)$_2$HTaOSi$^t$Bu$_2$CMe$_2$CH$_2$ (**61**). Unfortunately the crystallographic difficulties prevented extensive analysis of the bonding.

In contrast to related $\eta^1$-pyridine complexes of titanium, scandium and vanadium, treatment of **59** with pyridine afforded (silox)$_3$Ta($\eta^2$-(N,C)-py) (**62**-py), whose structural core is illustrated in Scheme 13. EHMO calculations employed to test trajectories for the approach of pyridine to the $d^2$ tantalum centre aided in rationalizing the observed $\eta^2$-geometry. If the pyridine approaches in the usual fashion, i.e. the N lone pair directed at the filled $d_{z^2}$ orbital of **59**, substantial 4e$^-$ repulsion develops, and the pyridine turns to bind as if it were an olefin. Olefin and acetylene complexes such as (silox)$_3$Ta($\eta^2$-$C_2H_4$) (**63**) and (silox)$_3$Ta($\eta^2$-$C_2Me_2$) (**64**) form readily as long as the substrate is small, and adduct generation is competitive with cyclometallation to **61**. As the ring distances in Scheme 13 attest, the pyridine functions as a decent $\pi$-acceptor when bound in the $\eta^2$-(N,C) conformation, and the organic fragment is best described as a diene. In essence, strong Ta—C and Ta—N $\sigma$-bonds are formed as the pyridine is bound as a metallaaziridene, and the oxidation state may be considered as $Ta^V$, similar to interpretations of early transition metal olefin binding as metalla-

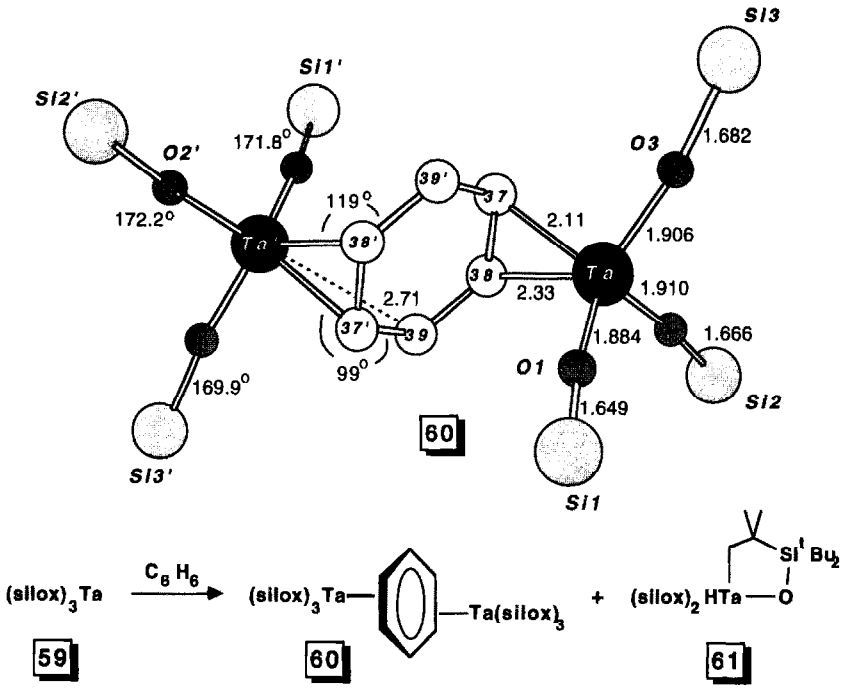


Fig. 7. Skeletal view of the core atoms pertaining to $[(silox)_3Ta]_2(\mu\text{-}C_6H_6)$ (**60**). The bridging group was disordered and modelled using standard constraints, hence bond distances and angles are not shown.

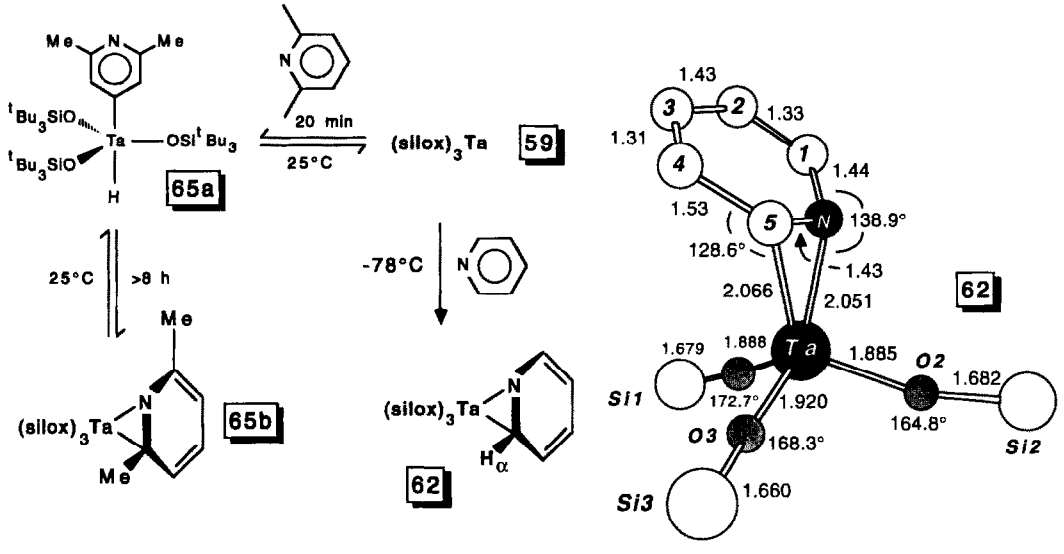


Scheme 13.

cyclopropane-like in character.[30] Considerable disruption of the ~35 kcal $mol^{-1}$ resonance energy of pyridine must result from the interaction. Related $\eta^2$-adducts were produced from 2-picoline, pyridazine and pyrimidine, but 2,6-lutidine yielded an alternative structure. Initially, oxidative addition of the *para*-CH bond occurred to afford $(silox)_3Ta(H)(2,6\text{-}Me_2\text{-}C_5H_2N)$ (**65a**), but equilibration with $(silox)_3Ta(\eta^2\text{-}(N,C)\text{-}2,6\text{-}NC_5H_3Me_2)$ (**65b**) was eventually observed. Formation of these $\eta^2$-heterocyclic adducts is proposed to occur via nucleophilic attack by **59** at the LUMO (predominantly C=N $\pi^*$) of the substrate. With 2,6-lutidine, attack is first directed at the next LUMO because of steric hindrance; subsequent hydride transfer produces pyridyl-hydride **65a**.

*Carbon monoxide cleavage.* Observation of carbon monoxide cleavage by $(silox)_3Ta$ (**59**) is by far

the most powerful example of its reductive potential.[30] The most widely accepted initial step of the Fischer–Tropsch (F–T) reaction is the dissociative adsorption of carbon monoxide (step 1, Scheme 14) to give a surface carbide ($C_s$) and oxide ($O_s$), a process modelled by the carbonylation of $(silox)_3Ta$ (**59**, eq. 32). Cleavage of CO by **59** afforded the dicarbide $[(silox)_3Ta]_2(\mu\text{-}C_2)$ (**66**), oxo $(silox)_3Ta{=}O$ (**67**), and ketenylidene $(silox)_3TaCCO$ (**68**). X-ray crystallographic, IR and Raman studies of **66** manifested a near-linear $\mu\text{-}C_2$ bridge ($\angle$ TaCC = 173 (3)°), a C=C double bond (1.37 (4) Å, $\nu$(C=C) = 1617 $cm^{-1}$) and typical TaC double bonds (1.95 (2) Å, $\nu$(Ta=C) = 709 $cm^{-1}$). EHMO calculations of a linear $\mu\text{-}C_2$-bridged $D_{3d}$ **66** indicated that the $e_{g2}$ HOMO ($^3A_{2g}$, $^1E_g$, $^1A_{1g}$) is ~80% Ta ($d_{xz}$, $d_{yz}$) and ~20% C ($p_x$, $p_y$). Magnetic susceptibility mesurements (2–300 K) were consistent with a large temperature independent susceptibility (25°C, $\mu_{eff}$ = 1.93 BM) and a singlet ground state, either $^1E_g$, $^1A_{1g}$, or one arising from a Jahn–Teller distortion of the $^1E_g$ level.

$$(silox)_3Ta\ (\mathbf{59}) \xrightarrow{(0.5+x)\,CO} (0.5-x)/2[(silox)_3Ta]_2(\mu\text{-}C_2)\ (\mathbf{66}) + 0.5\,(silox)_3Ta{=}O\ (\mathbf{67}) + x(silox)_3TaCCO\ (\mathbf{68}) \quad (32)$$

The most plausible overall mechanism for the formation of dicarbide **66**, compiled from numerous labelling, kinetic and modelling studies, is shown in Scheme 15. Critical steps in the sequence are as follows: (1) $(silox)_3Ta$ (**59**) binds CO to form an unstable, pseudo-tetrahedral, paramagnetic adduct, $(silox)_3TaCO$ (**59**-CO); (2) in donor solvents (*S*), **59**-CO is trapped and stabilized by solvent (−78°C) as $(silox)_3STaCO$ (*S*-**59**-CO); (3) either aggregation of *S*-**59**-CO and equilibrium amounts of **59**-CO (a), dimerization of **59**-CO (b), or a disproportionation of **59**-CO to **59** and **59**-$(CO)_2$, which then quickly recombine (c), generates a red precipitate (−78° to −50°C), designated as $[(silox)_3TaCO]_n$ ($[\mathbf{59}\text{-CO}]_n$, $n$ = 2); (4) either (b) or (c) leads to $[\mathbf{59}\text{-CO}]_n$ in non-donor solvents; (5) degradation of $[\mathbf{59}\text{-CO}]_n$, possibly through cleavage of the four-membered ring (~5°C), produces the ketenylidene, $(silox)_3Ta{=}C{=}C{=}O$ (**68**), and the oxo, $(silox)_3Ta{=}O$ (**67**); (6) another $(silox)_3Ta$ (**59**) then deoxygenates ketenylidene **68**, (~5°C), probably via intermediate adduct $(silox)_3Ta{=}C{=}C{-}O{-}Ta(silox)_3$ (**68**·**59**), to afford oxo **67** and a transient vinylidene, $(silox)_3Ta{=}C{=}C$: (**59**-$C_2$), that electronically resembles CO; (7) in the dicarbide-forming last step, a final $(silox)_3Ta$ (**59**) unit scavenges the vinylidene (**59**-$C_2$), resulting in $[(silox)_3Ta]_2(\mu\text{-}C_2)$ (**66**).

If one accepts the premise that early metal complexes exhibit reactivity commensurate with late transition metal/metal oxide F–T systems (e.g. $Fe_2O_3$ or $Co_2O_3$ on $Al_2O_3$ or $SiO_2$) that operate at higher temperatures and pressures, some important conclusions may be drawn. Heterogeneous models

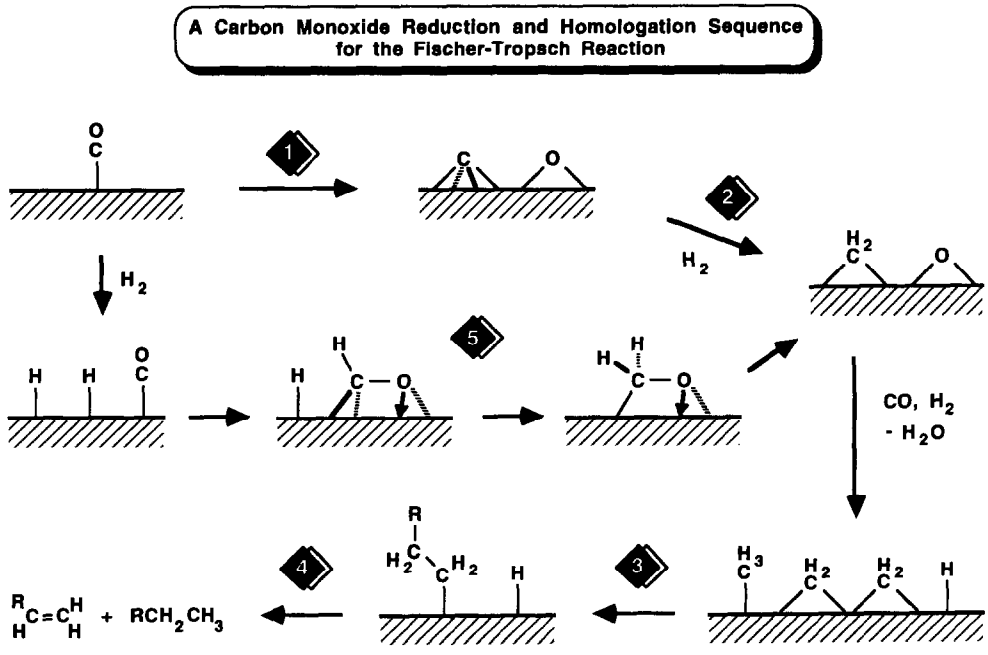


Scheme 14.

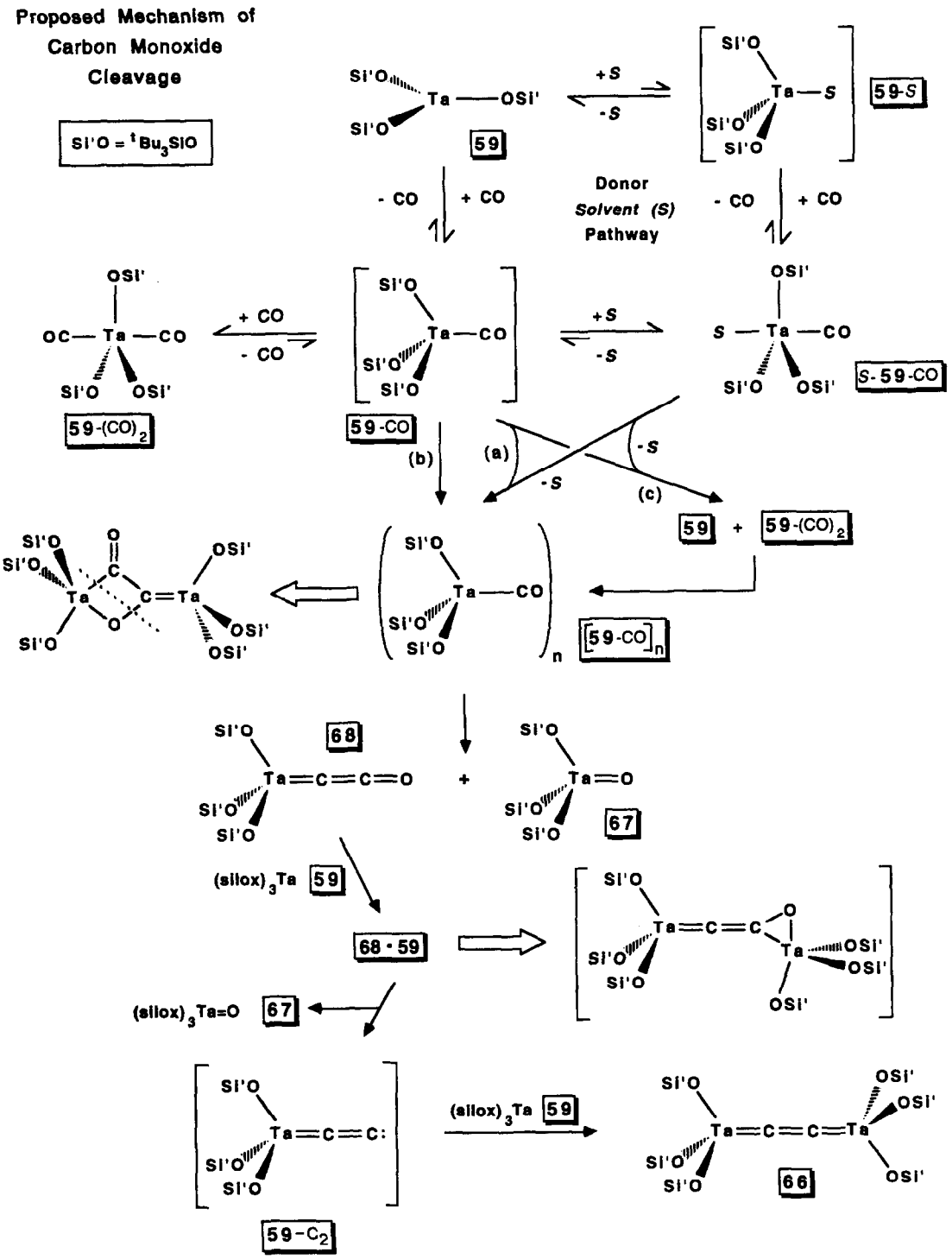


Scheme 15.

suggest that an emsemble of five atoms is needed for the dissociative adsorption of CO, but only two tantalums are involved in the formation of ketenylidene $(silox)_3Ta{=}C{=}C{=}O$ (**68**) and oxo **67**; an additional two tantalums are involved in deoxygenation of **68**. The only *requirement* for CO dissociation is either six (to $C^{4-}$ and $O^{2-}$) or four electrons (to 1/2 $C_2^4$ and $O^{2-}$); the number of metals capable of supplying this quantity may vary. The $d^2$ $(silox)_3Ta$ (**59**) molecule is a potent reductant, yet is electrophilic, a unique combination that enables homogeneous CO dissociation. The heterogeneous dissociative adsorption of CO has been experimentally verified, yet intriguing questions

regarding the mechanism(s) by which adsorbed CO cleaves to give $C_s$ and $O_s$ remain.

*Oxidative additions*: $(silox)_3HTaEHPh$. Over 50 different substrates have been studied in regard to the oxidative addition chemistry of $(silox)_3Ta$ (**59**) during the past 11 years, and some recent results involving pnictide substrates represent intriguing examples.[34] As Scheme 16 depicts, exposure of **59** to 1.0 equiv. $PhEH_2$ in benzene (E = N, P; 25°C) or toluene (E = As, −76°C) afforded the thermally unstable, pnictide hydrides $(silox)_3HTaEHPh$ (**69**-EHPh, E = N, P, As). Qualitative rates of oxidative addition reflected the expected order (AsH ≫ PH > NH) based on thermodynamic influences on the process, although arsinide-hydride formation was decidedly swifter than NH and PH addition.

Subsequent first-order 1,2-$H_2$-elimination from **69**-EHPh produced the corresponding $(silox)_3Ta{=}EPh$ derivatives: colourless imide $(silox)_3Ta{=}NPh$ (**70**-NPh, $k_N(24.8(3)°C) = 3.8(2) \times 10^{-5}$ $s^{-1}$), red phosphinidene $(silox)_3Ta{=}PPh$ (**70**-PPh, $^{31}P$ NMR $\delta$ 334.6, $k_P(24.8(3)°C) = 2.6(1) \times 10^{-6}$ $s^{-1}$), and green arsinidene, $(silox)_3Ta{=}AsPh$ (**70**-AsPh, $k_{As}(-76(1)°C) = 1.4(2) \times 10^{-3}$ $s^{-1}$). When a $\Delta S^{\ddagger} \sim -10$ eu was assumed for **70**-AsPh formation, relative rates at 25°C revealed tremendous differences between the arsinidene and the remaining pnictidenes: As $(2.6 \times 10^7) \gg$ N (15) > P (1). The rates contradict thermodynamic influences that suggest As > P > N, and may reflect the different geometric constraints critical to the transition state for each 1,2-$H_2$-elimination event. The extremely swift formation of **3**-AsPh may represent a mechanistic change, or may show the dramatically increased propensity to generate low-valent pnictide fragments by the heavier elements. Single crystal, X-ray structural studies of $(silox)_3Ta{=}EPh$ (**70**-PPh, **70**-AsPh) revealed an isomorphic relationship. The complexes possess bent phosphinidene (**70**-PPh: $\angle$Ta—P—C = 110.2(4)°, $d$(Ta=P) = 2.317(4) Å) and arsinidene (**70**-AsPh: $\angle$Ta—As—C = 107.2(4)°, $d$(Ta=As) = 2.428(2) Å) fragments with relatively short Ta=E distances, consistent with one strong $\pi$-bond, and a pnictide-localized "lone-pair" orbital.

*Three-coordinate tungsten*: $(silox)_2W{=}N^tBu$

Continuing with the theme of low-coordinate, low-valent silox derivatives, an entry into group 6 was established via the silanolysis of Nugent's $(^tBuNH)_2W(=N^tBu)_2$ to yield $(silox)_2W(=N^tBu)_2$ (**71**, eq. 33).[35] Upon treatment with HCl, **71** was converted to $(silox)_2Cl_2W{=}N^tBu$ (**72**, eq. 34), which was subsequently reduced with excess mag-

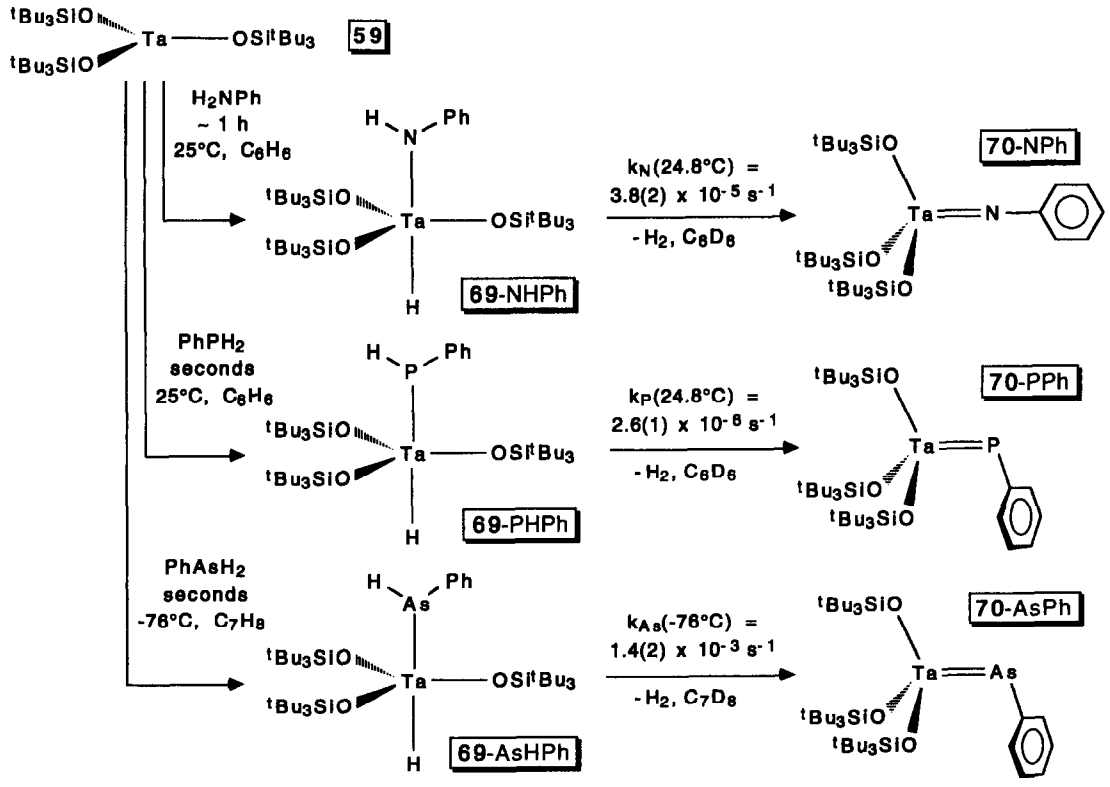


Scheme 16.

nesium in $Et_2O$ to give emerald green, 3-coordinate

$$(^tBuNH)_2W(=N^tBu)_2 + 2(silox)H \xrightarrow[>3\,d,\,90\,^\circ C]{benzene} (silox)_2W(=N^tBu)_2 + 2\,^tBuNH_2 \quad (33)$$

**71**

$$(silox)_2W(=N^tBu)_2 + 3HCl \xrightarrow[3.5\,d,\,110\,^\circ C]{benzene} (silox)_2Cl_2W{=}N^tBu + [^tBuNH_3]Cl \quad (34)$$

**72**

$(silox)_2W = N^tBu$ (**73**) in 78% yield (Scheme 17). An X-ray crystallographic study confirmed the anticipated planar geometry of **73**, although the $^t$Bu groups of the silox ligands were disordered. The W=N distance is somewhat short (1.658(17) Å), while each W—O—Si angle (169.7(10), 177.8(8)°) and the W=N—C angle (175.3(16)°) are nearly linear. The bonding in $d^2$ **73** is reminiscent of $(silox)_3Ta$ (**59**) and Schrock's tris-imidoosmium derivative, $Os(=N\text{-}2,6\text{-}^iPrC_6H_3)_3$.[36] In each planar $d^2$ complex, the full complement of $\pi$-bonding by the siloxide and imido donors is available with the exception of one non-bonding ligand $p$-orbital combination.

The addition of 2-butyne and ethylene to **73** afforded the adducts $(silox)_2(\eta^2\text{-MeC}{\equiv}\text{CMe})W{=}N^tBu$ (**74**) and $(silox)_2(\eta^2\text{-}C_2H_4)W{=}N^tBu$ (**75**), respectively.[35] The activation energy for rotation of the $C_2H_4$ unit of the latter is 15.3 kcal mol$^{-1}$ (69°C), consistent with a strong binding to the $W^{IV}$ centre in the orientation shown. Optimal $\pi$-bonding is expected in this conformation by comparison to numerous $(RO)_2(R'N{=})W{=}CHR''$ species prepared by Schrock *et al.*[37] The oxidative addition of dihydrogen (3 atm) to **73** cleanly produced $(silox)_2H_2W{=}N^tBu$ (**76**), as evidenced by its $^1$H NMR ($\delta(WH_2)$ 18.38, $J_{WH}$ = 131 Hz) spectrum, but removal of the $H_2$ atmosphere induced the generation of substantial amounts of the red cyclometallated derivative, $(silox)(^tBuN{=})HWOSi^tBu_2CMe_2CH_2$ (**77**), independently prepared via thermolysis of **73** in cyclohexane at 100°C for 5 days.[38] Detailed investigations of this chemistry are still under way.

## METAL–METAL BONDED COMPLEXES

### $[(silox)_2TaH_2]_2$

*Synthesis.* Since silox was so effective at supporting unusual, low oxidation state early transition metal centres, it seemed likely that metal–metal bonded complexes could be readily prepared. Scheme 18 illustrates how reduction of $(silox)_2TaCl_3$ (**13**) in the presence of $H_2$ yielded the orange $D_{2d}$ dimer, $[(silox)_2TaH_2]_2$ (**78**, 83%).[39,40] The tetrahydride is incredibly robust, melting at 180°C and distilling at 220°C ($10^{-4}$ torr). A single crystal X-ray diffraction experiment and various spectroscopic investigations showed that **78** possesses an unbridged Ta—Ta bond of 2.720(4) Å that connects two interlocked trigonal bipyramids containing axial hydrides and basal silox groups.

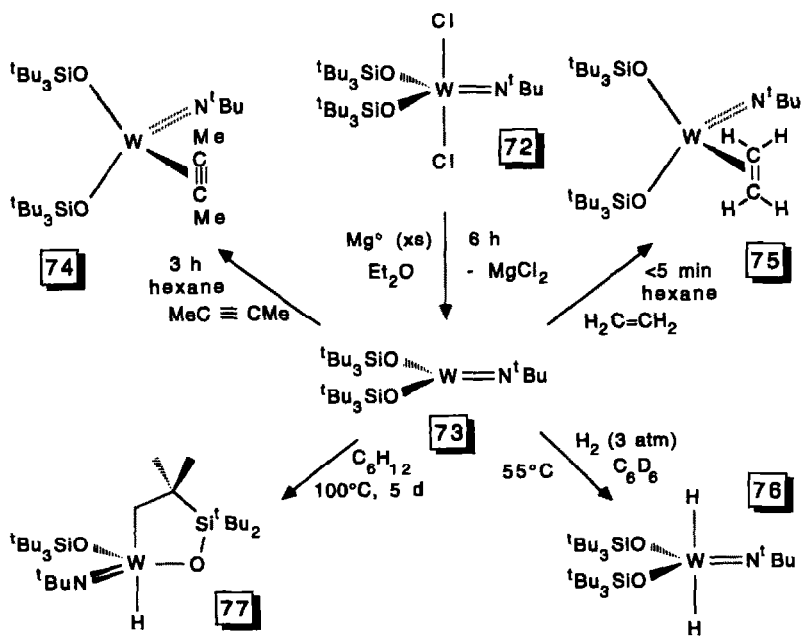


Scheme 17.

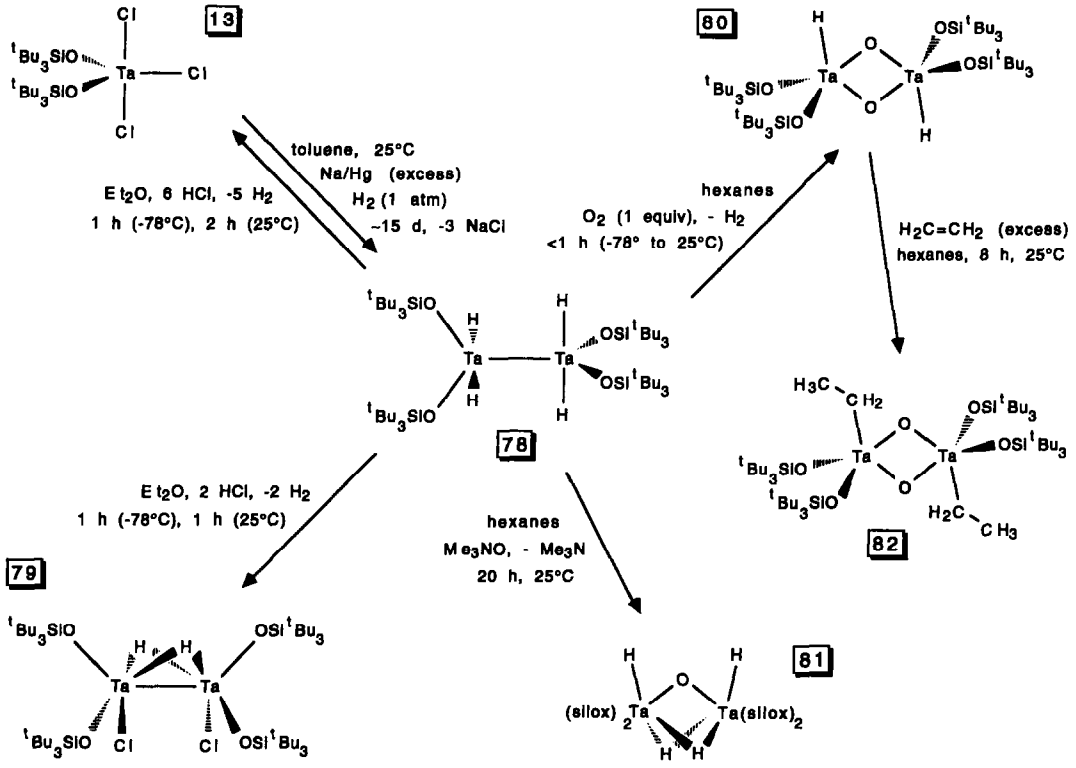


Scheme 18.

The tetrahydride **78** served as a critical starting material for the preparation of related dimeric complexes. Careful addition of 2.0 equiv. HCl to **78** permitted the synthesis of purple $[(silox)_2TaCl]_2(\mu\text{-}H)_2$ (**79**), a complex postulated to contain bridging hydrides on the basis of infrared studies and comparisons to related Cp-containing $Ta^{IV}$ dimers. Oxidation of the $Ta_2$ unit occurred smoothly with 1.0 equiv. of $O_2$, affording the bis-$\mu$-oxo dimer, $[(silox)_2TaH]_2(\mu\text{-}O)_2$ (**80**), and concomitant $H_2$, while a single O-atom was admitted via $Me_3NO$ to produce the $\mu$-oxo dimer, $[(silox)_2TaH]_2(\mu\text{-}H)_2(\mu\text{-}O)$ (**81**). Compound **81** exists in two $(\mu\text{-}H)_2$-bridged forms that rapidly interconvert via $[(silox)_2TaH_2]_2(\mu\text{-}O)$, as determined from variable temperature $^1H$ and $^{29}Si\ \{^1H\}$ NMR experiments. Exposure to ethylene derivatized **80** via double insertion, resulting in $[(silox)_2TaEt]_2(\mu\text{-}O)_2$ (**82**).

CO *hydrogenation, deoxygenation and* C—C *coupling*. In 1926, Fischer and Tropsch postulated a mechanism for the conversion of synthesis gas ($CO/H_2$) to hydrocarbons that incorporates three critical steps illustrated in Scheme 14 (*vide supra*): (1) CO is deoxygenated; (2) H-transfer to surface carbides or $CO_{ads}$ produces surface methylene groups; and (3) C—C bond formation occurs through oligomerization of $(CH_2)_{ads}$. The homogeneous system discussed below, which utilizes only M—H and CO, exhibits each crucial transformation.

As Scheme 19 depicts,[40] $D_{2d}$ $[(silox)_2TaH_2]_2$ (**78**) severed the carbon–oxygen bond of CO while transferring two hydrides to form the $\mu$-$CH_2$ species, $[(silox)_2HTa]_2(\mu\text{-}O)(\mu\text{-}CH_2)$ (**83**), thus modelling $(CH_2)_{ads}$. Reformation of the C=O bond upon addition of another equiv. of CO generated a $\mu$-formyl/$\mu$-formaldehyde complex, $[(silox)_2HTa](\mu\text{-}CHO)(\mu\text{-}CH_2O)[Ta(silox)_2]$ (**84**), with the original carbonyl carbon residing in the $\mu$-CHO. Mild, thermal deoxygenation of both bridging groups resulted in C—C bond formation, affording the $\mu$-ethylidene, $[(silox)_2Ta]_2(\mu\text{-}O)_2(\mu\text{-}CHMe)$ (**85**), with the original carbon residing in the bridge. When **78** or formylformaldehyde **84** was exposed to 1 atm CO, a third carbonyl was reduced to provide $[(silox)_2Ta]_2(\mu\text{-}O)(\mu\text{-}CH_2O)(\mu\text{-}OCH{=}CH)$ (**86**). As shown via $^{13}C$ labelling, the middle position of the 3-atom enolate bridge (**86**) is comprised of the latter carbon, which is attached to the deoxygenated formyl carbon of **84**.

When protonated, these complexes generated a nearly full complement of $C_1$ and $C_2$ hydrocarbons and oxygenates, Fischer–Tropsch (F–T) products typically produced under hydrogenation conditions: $CH_4$ was released from **83**; $C_2H_6$ from **85**; $CH_3OH$ from **84** and **86**; $H_3CCHO$ from **86**. In

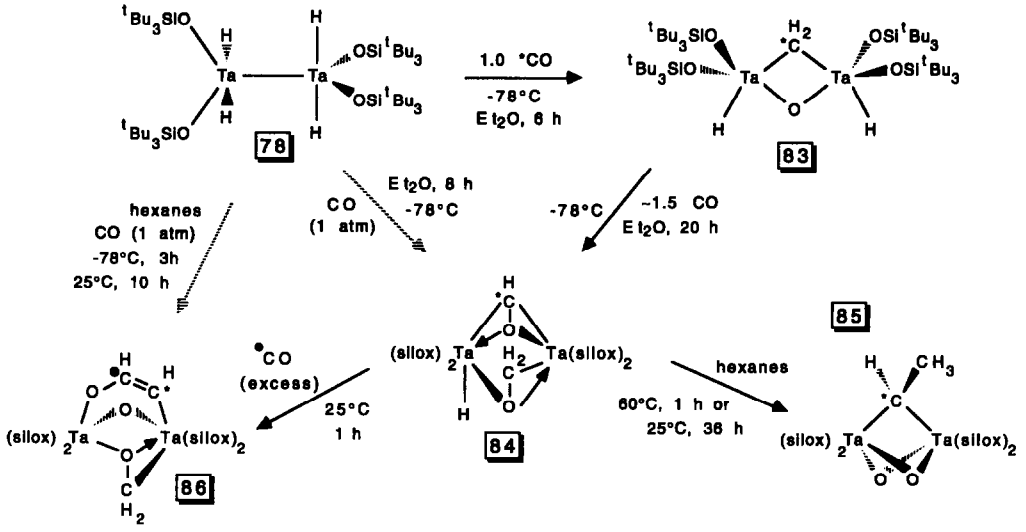


Scheme 19.

addition to modelling transformations critical to the F–T sequence, two alternative views of the heterogeneous process may be proffered. Since **83** is formed directly, the generation of $(CH_2)_{ads}$ via H-transfer concomitant with or prior to C—O bond scission must still be considered as a viable mechanism; the dissociative adsorption of CO may not be necessary. Noting that a C—O bond has been broken, reformed and broken again in the conversion of **83** to **85**, heterogeneous oxygenated surfaces may serve as reservoirs for CH, $CH_2$ and $CH_3$ functionalities via $(OCH)_{ads}$, $(OCH_2)_{ads}$ and $(OCH_3)_{ads}$ etc. Hydrocarbon units on actual F–T surfaces should not be considered constrained to be metal-bound.

$H_2$ *exchange*. In the course of examining the carbonylations of $[(silox)_2TaH_2]_2$ (**78**), two distinct hydrogen exchange events were observed.[40] Exchange with $D_2$ to give the isotopomers $(silox)_4Ta_2H_3D$ (**78**-D), $(silox)_4Ta_2H_2D_2$ (**78**-$D_2$), $(silox)_4Ta_2HD_3$ (**78**-$D_3$) and $(silox)_4Ta_2D_4$ (**78**-$D_4$) occurred rapidly (eq. 35), and all but the last derivative were observed via resonances shifted due to an NMR isotope effect. Magnetization transfer $^1H$ NMR experiments conducted at various tem-

$$\underset{\mathbf{78}}{[(silox)_2TaH_2]_2} + H_2^* \xrightarrow{\text{benzene-}d_6} \underset{\mathbf{78}^*}{(silox)_4Ta_2H_3H^*} + HH^* \quad (35)$$

peratures showed a rapid second-order exchange of $H_2^*$ with **78** [e.g. at 50°C, $k = 9.2(3) \times 10^2$ $M^{-1}$ $s^{-1}$; at 100°C, $k = 3.3(2) \times 10^3$ $M^{-1}$ $s^{-1}$; $\Delta H^{\ddagger} = 6.0(1)$ kcal $mol^{-1}$, $\Delta S^{\ddagger} = -27(3)$ eu]. The activation parameters are consistent with a $\sigma$-bond metathesis pathway for exchange.

When **78** and **78**-$D_4$ are placed in solution, a statistical distribution of isotopomers gradually forms (eq. 36). Several features to the exchange are apparent: (1) exchange occurs sporadically, with $k_{obs}$ that vary by $\sim 10$ with the same concentration of **78**/**78**-$D_4$; (2) it is *roughly* first order in

$$\underset{\mathbf{78}}{(silox)_4Ta_2H_4} + \underset{\mathbf{78}\text{-}D_4}{(silox)_4Ta_2D_4} \rightleftharpoons \underset{\mathbf{78}\text{-}D}{(silox)_4Ta_2H_3D} + \underset{\mathbf{78}\text{-}D_2}{(silox)_4Ta_2H_2D_2} + \underset{\mathbf{78}\text{-}D_3}{(silox)_4Ta_2HD_3} \quad (36)$$

[**78**/**78**-$D_4$]; (3) no acid or base catalysis is evident; (4) a non-pairwise exchange of siloxes occurs at similar rates; (5) hydride exchange is not mediated by $HOSi^tBu_3$; (6) free radical initiators and scavengers unreactive with **78** do not affect the rate. Although the exchange rates are difficult to model using parameters obtained from the magnetization transfer experiments, we still tentatively favour catalysis by trace $H_2/D_2/HD$ as the most probable pathway to explain eq. (36), but there are many aspects to this hydride exchange reaction that remain a puzzle.

*Carbide formation via* CO *dissociation across a* W=W *bond*

As Scheme 20 indicates, $(silox)_2ClW{=}WCl(silox)_2$ (**87**, $C_2$ symmetry), prepared in 75% yield from Na(silox) and $NaW_2Cl_7(THF)_5$, served

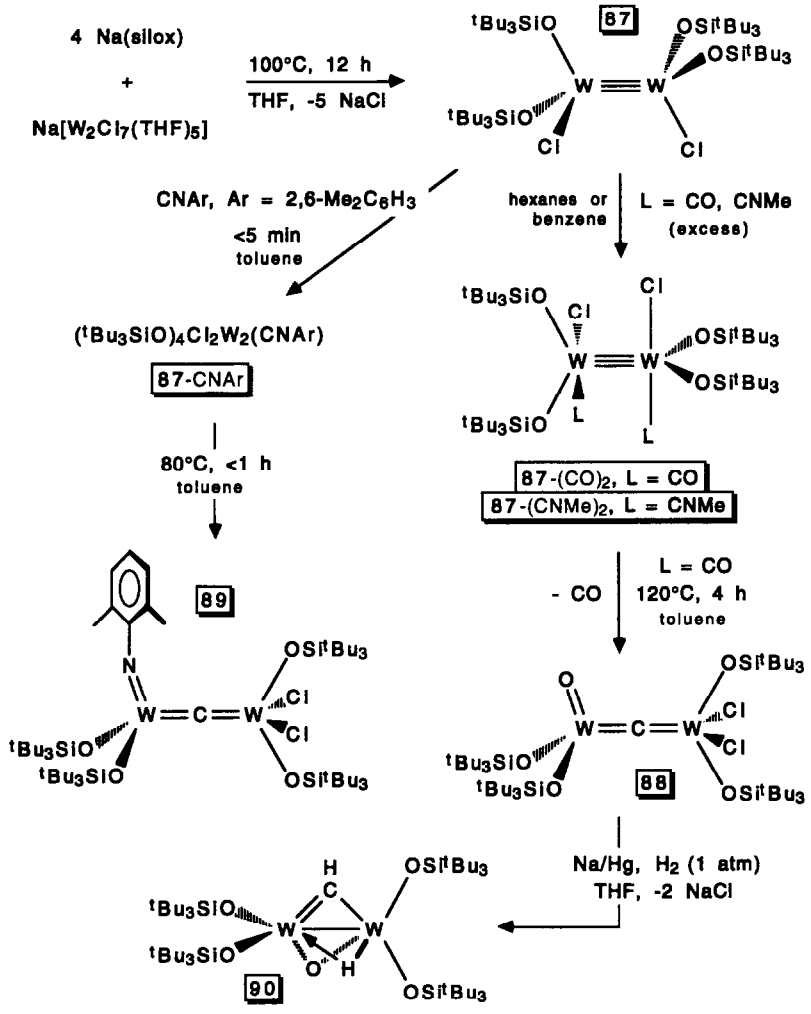


Scheme 20.

as a precursor to $C_2$ dicarbonyl (interlocked tbps), $C_2$ bis-methylisonitrile, carbonyl-methylisonitrile and arylisonitrile adducts: $[(silox)_2Cl(L)W]_2$ (L = CO, **87**-$(CO)_2$, 95%; L = CNMe, **87**-$(CNMe)_2$, 79%), $(silox)_2Cl(CO)W{=}W(CNMe)Cl(silox)_2$ (**87**-CO,CNMe), $(silox)_4W_2Cl_2(CNAr)$ (**87**-CNAr, Ar = 2,6-$Me_2C_6H_3$).[41] Thermolysis of **1**-$(CO)_2$ for 4 h at 120°C in toluene produced 0.87 equiv. of CO and oxo-$\mu$-carbide $(silox)_2(O)W{=}C{=}WCl_2(silox)_2$ (**88**, 70%). Once again, reduced metal centres, this time a pair of formally $W^{III}$ atoms, proved effective at cleaving the 257 kcal $mol^{-1}$ bond of carbon monoxide. Rough kinetics support an intramolecular mechanism involving CO loss from **87**-$(CO)_2$, followed by scission of the ligated carbonyl. In a presumably similar process, generation and subsequent degradation of transient **87**-CNAr led to the formation of imido-$\mu$-carbide $(silox)_2(ArN)W{=}C{=}WCl_2(silox)_2$ (**89**, 58%). While the crystal structure of **88** manifested a pronounced disorder in the orientation of the W=O unit relative to the neighbouring square pyramid, the crystal structure of imido-$\mu$-carbide **89** was markedly better despite the usual silox disorder, revealing a rough tetrahedral/square pyramidal geometry with an asymmetric $W_2C$ bridge: $d$(W(tet)—C) = 1.994(17) Å, $d$(W(sq pyr)—C) = 1.769(17) Å, $\angle$WCW = 176.0(12)°.

Reduction of **88** with Na/Hg under 1 atm $H_2$ yielded $[(silox)_2W]_2(\mu\text{-CH})(\mu\text{-O})(\mu\text{-H})$ (**90**, 44%). The reduction cleavage of CO requires $6e^-$, exactly the number provided by the $(W{=}W)^{6+}$ core; the scission of CO represents a discrete homogeneous analogue to the putative first step in the Fischer–Tropsch process, the dissociative adsorption of CO (*vide supra*). These observations complement those of Chisholm *et al.*, who have also observed CO cleavage mediated by other $W{=}W^{6+}$ alkoxides.[42]

## FUTURE EFFORTS

After 13 years of investigating the chemistry of early transition metal alkoxide and siloxide complexes, there remains a considerable amount to be discovered, and we are still happily engaged in exploration. It is clear that silox is the most robust of the hindered ligands investigated, and certainly the most versatile. Nonetheless, variations of this theme present an intriguing target for future studies; perhaps the $Cy_3SiO$ ligand will instill an even greater degree of steric shielding about a metal centre, permitting better control over metathetical procedures. Related heteroatom ligands, most notably $^tBu_3SiNH$,[43–46] are already being applied in several areas. We have yet to show that one of these systems can be useful in some catalytic process, but will continue to seek potential utilizations of bulky alkoxide/siloxide-derived compounds, provided the chemistry is interesting. Finally, we are proceeding to push the limits of silox applicability to the right side of the periodic table. Who knows *exactly* where the next 13 years are likely to lead us; all we know is that it will definitely be intriguing.

*Acknowledgements*—It is my pleasure to thank my principal co-workers on the various projects for their dedication, perseverance and skill, for without their hard work I would be pumping gas somewhere. Consult the references for the efforts of these individuals: Dr Timothy V. Lubben, Dr Robert E. LaPointe, Dr Gregory S. Ferguson, Dr Steven M. Baxter, Dr David R. Neithamer, Dr Katharine J. Covert, Dr Robert Toreki, Dr Mark M. Banaszak Holl, Daniel F. Eppley, Dr Christopher P. Schaller, Dr Rebecca L. Miller and Jeffrey B. Bonanno. I truly appreciate the many collaborations evident throughout the work described, but reserve special thanks for Dr Gregory Van Duyne, Prof. Barry K. Carpenter, and the collective help of the Hoffmann group. The majority of this work has been supported by funds from the National Science Foundation, who I gratefully acknowledge. Cornell University, the Air Force Office of Scientific Research and the ACS Petroleum Research Fund are also thanked for their contributions.

## REFERENCES

1. J. P. Collman, L. S. Hegedus, J. R. Norton and R. G. Finke, *Principles and Applications of Organotransition Metal Chemistry*. University Science Books, Mill Valley, CA (1987).
2. D. C. Bradley and M. H. Chisholm, *Acc. Chem. Res.* 1976, **9**, 273.
3. M. F. Lappert, P. P. Power, A. R. Sanger and R. C. Srivastava, *Metal and Metalloid Amides*. Ellis Horwood, Chichester (1980).
4. C. A. Tolman, *Chem. Rev.* 1977, **77**, 313.
5. L. Chamberlain, J. C. Huffman, J. Keddington and I. P. Rothwell, *J. Chem. Soc., Chem. Commun.* 1982, 805.
6. B. D. Steffey, P. E. Fanwick and I. P. Rothwell, *Polyhedron* 1990, **9**, 963.
7. O. W. Steward and D. R. Fussaro, *J. Organomet. Chem.* 1977, **129**, C28.
8. S. Shambayatei, J. F. Blake, S. G. Wierschke, W. L. Jorgensen and S. L. Schreiber, *J. Am. Chem. Soc.* 1990, **112**, 697; 6155.
9. (a) K. J. Covert, P. T. Wolczanski, S. A. Hill and P. J. Krusic, *Inorg. Chem.* 1992, **31**, 66; (b) K. J. Covert and P. T. Wolczanski, *Inorg. Chem.* 1989, **28**, 4565.
10. P. D. Bartlett and E. B. Lefferts, *J. Am. Chem. Soc.* 1955, **77**, 2804.
11. L. Syper, *Rocz. Chem.* 1973, **47**, 433.
12. T. V. Lubben, P. T. Wolczanski and G. D. Van Duyne, *Organometallics* 1984, **3**, 977.
13. R. E. LaPointe, P. T. Wolczanski and G. D. Van Duyne, *Organometallics* 1985, **4**, 1810.
14. M. Nandi, D. Rhubright and A. Sen, *Inorg. Chem.* 1990, **29**, 3066–3068.
15. E. M. Dexheimer, L. Spialter and L. D. Smithson, *J. Organomet. Chem.* 1975, **102**, 21–27.
16. K. J. Covert, Ph.D. Thesis, Cornell University (1991).
17. M. Weidenbruch, C. Pierrard and H. Pesel, *Z. Naturforsch.* 1978, **33B**, 1468–1471.
18. Alternatively prepared from Na(silox) and $Cl_3VO$: R. Toreki and P. T. Wolczanski, unpublished results.
19. S. Patai and Z. Rappaport (Eds), *The Chemistry of Organic Silicon Compounds*. Wiley and Sons, New York (1989).
20. (a) V. H. Hellmann, J. Bader, H. Brikner and O. Schumacher, *Liebigs Ann. Chem.* 1962, **659**, 49; (b) G. S. Ferguson and P. T. Wolczanski, *Organometallics* 1985, **4**, 1601.
21. S. M. Baxter, G. S. Ferguson and P. T. Wolczanski, *J. Am. Chem. Soc.* 1988, **110**, 4231.
22. S. M. Baxter and P. T. Wolczanski, *Orgnometallics* 1990, **9**, 2498.
23. N. E. Shore, L. S. Benner and B. E. LaBelle, *Inorg. Chem.* 1981, **20**, 3200.
24. (a) G. S. Ferguson, P. T. Wolczanski, L. Párkányi and M. C. Zonnevylle, *Organometallics* 1988, **7**, 1967; (b) G. S. Ferguson and P. T. Wolczanski, *J. Am. Chem. Soc.* 1986, **108**, 8293.
25. (a) T. V. Lubben and P. T. Wolczanski, *J. Am. Chem. Soc.* 1987, **109**, 424; (b) T. V. Lubben and P. T. Wolczanski, *J. Am. Chem. Soc.* 1985, **107**, 701.
26. (a) M. M. Banaszak Holl, M. Kersting, B. D. Pendley and P. T. Wolczanski, *Inorg. Chem.* 1990, **29**, 1518; (b) M. M. Banaszak Holl, P. T. Wolczanski and G. D. Van Duyne, *J. Am. Chem. Soc.* 1990, **112**, 7989; (c) R. L. LaDuca and P. T. Wolczanski, *Inorg. Chem.* 1992, **31**, 1311.
27. M. M. Banaszak Holl and P. T. Wolczanski, *J. Am. Chem. Soc.* 1992, **114**, 3854.
28. F. Feher, S. Wells and J. Hemminger, personal communication.
29. P. G. Gassman, D. W. Macomber and J. W. Herschberger, *Organometallics* 1983, **2**, 1470.

30. (a) D. R. Neithamer, R. E. LaPointe, R. A. Wheeler, D. S. Richeson, G. D. Van Duyne and P. T. Wolczanski, *J. Am. Chem. Soc.* 1989, **111**, 9056; (b) R. E. LaPointe, P. T. Wolczanski and J. F. Mitchell, *J. Am. Chem. Soc.* 1986, **108**, 6382.
31. K. J. Covert, D. R. Neithamer, M. C. Zonnevylle, R. E. LaPointe, C. P. Schaller and P. T. Wolczanski, *Inorg. Chem.* 1991, **30**, 2494.
32. J. S. Wood, *Inorg. Chem.* 1968, 7, 852.
33. D. R. Neithamer, L. Párkányi, J. F. Mitchell and P. T. Wolczanski, *J. Am. Chem. Soc.* 1988, **110**, 4421.
34. J. B. Bonanno, P. T. Wolczanski and E. B. Lobkovsky, *J. Am. Chem. Soc.* 1994, **116**, 11159.
35. D. F. Eppley, P. T. Wolczanski and G. D. Van Duyne, *Angew. Chem.* 1991, **103**, 616; *Angew. Chem. Int. Ed. Engl.* 1991, **30**, 584.
36. (a) M. H. Schofield, T. P. Kee, J. T. Anhaus, R. R. Schrock, K. H. Johnson and W. M. Davis, *Inorg. Chem.* 1991, **30**, 3595; (b) J. T. Anhaus, T. P. Kee, M. H. Schofield and R. R. Schrock, *J. Am. Chem. Soc.* 1990, **112**, 1642.
37. R. R. Schrock, R. T. DePue, J. Feldman, K. B. Yap, D. C. Yang, W. M. Davis, L. Park, M. DiMare, M. Schofield, J. Anhaus, E. Walborsky, E. Evitt, C. Krüger and P. Betz, *Organometallics* 1990, **9**, 2262.
38. D. F. Eppley, P. T. Wolczanski, unpublished results.
39. R. E. LaPointe, P. T. Wolczanski, *J. Am. Chem. Soc.* 1986, **108**, 3535.
40. (a) R. L. Miller, R. Toreki, R. E. LaPointe, P. T. Wolczanski, G. D. Van Duyne and D. C. Roe, *J. Am. Chem. Soc.* 1993, **115**, 5570; (b) R. Toreki, R. E. LaPointe and P. T. Wolczanski, *J. Am. Chem. Soc.* 1987, **109**, 7558.
41. R. L Miller, P. T. Wolczanski and A. L. Rheingold, *J. Am. Chem. Soc.* 1993, **115**, 10422.
42. (a) M. H Chisholm, C. E. Hammond, V. J. Johnston, W. E. Streib and J. C. Huffman, *J Am. Chem. Soc.* 1992, **114**, 7056; (b) M. H. Chisholm, B. W. Eichorn, K. Folting, J. C. Huffman, C. D. Ontiveros, W. E. Streib and W. G. Van Der Sluys, *Inorg. Chem.* 1987, **26**, 3182.
43. (a) C. C. Cummins, S. M. Baxter and P. T. Wolczanski, *J. Am. Chem. Soc.* 1988, **110**, 8731; (b) C. C. Cummins, G. D. Van Duyne, C. P. Schaller, P. T. Wolczanski, *Organometallics* 1991, **10**, 164; (c) C. P. Schaller, J. B. Bonanno and P. T. Wolczanski, *J. Am. Chem. Soc.* 1994, **116**, 4133.
44. C. C. Cummins, C. P. Schaller, G. D. Van Duyne, P. T. Wolczanski, E. A.-W. Chan and R. Hoffmann, *J. Am. Chem. Soc.* 1991, **113**, 2985.
45. C. P. Schaller and P. T. Wolczanski, *Inorg. Chem.* 1993, **32**, 13.
46. J. L. Bennett and P. T. Wolczanski, *J. Am. Chem. Soc.* 1994, **116**, 2179.